Cell Reports

Article

The Nrf2-Keap1 pathway is activated by steroid hormone signaling to govern neuronal remodeling

Graphical abstract

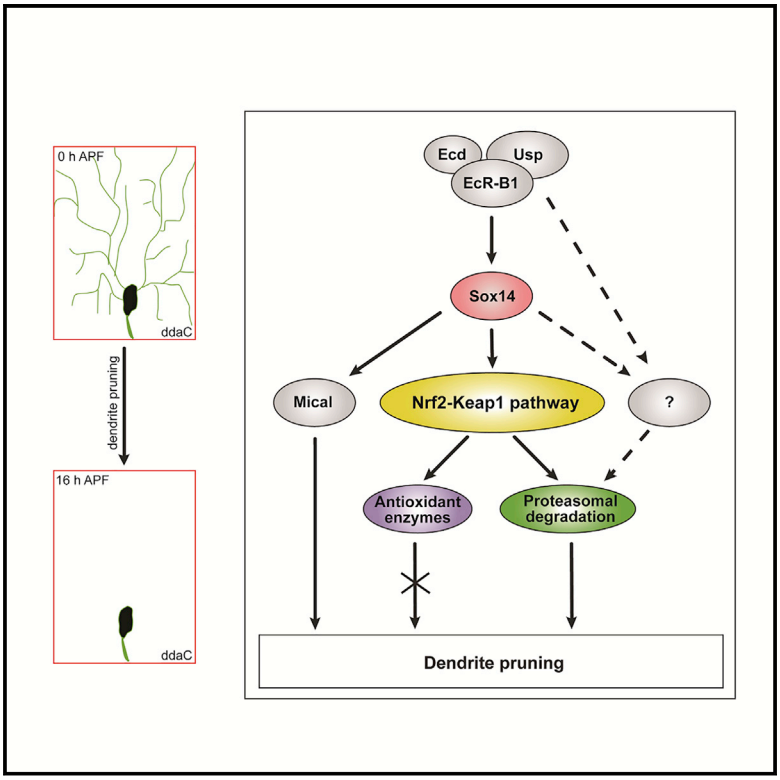

Authors

Liang Yuh Chew, Heng Zhang, Jianzheng He, Fengwei Yu

Correspondence

fengwei@tll.org.sg

In brief

Chew et al. uncover a critical role of the conserved Nrf2-Keap1 pathway in neuronal pruning during development. Nrf2-Keap1 signaling is activated via cytoplasmic-to-nuclear translocation of CncC/Nrf2, dependent on importin and ecdysone signaling. The pathway regulates pruning independent of its canonical antioxidant response pathway, acting instead through a proteasomal degradation pathway.

Highlights

- The conserved Nrf2-Keap1 pathway governs dendrite pruning of mechanosensory neurons
- Nrf2-Keap1 pathway is activated by ecdysone signaling prior to dendrite pruning
- Nrf2-Keap1 pathway is activated via a cytoplasmic-to-nuclear translocation of CncC
- Nrf2-Keap1 pathway regulates pruning via proteasomal but not antioxidant function

Chew et al., 2021, Cell Reports *36*, 109466
August 3, 2021
https://doi.org/10.1016/j.celrep.2021.109466

CellPress

Cell Reports

CellPress
OPEN ACCESS

Article

The Nrf2-Keap1 pathway is activated by steroid hormone signaling to govern neuronal remodeling

Liang Yuh Chew,[1,2,3] Heng Zhang,[1,3] Jianzheng He,[1] and Fengwei Yu[1,2,4,*]
[1]Temasek Life Sciences Laboratory, 1 Research Link, National University of Singapore, Singapore 117604, Singapore
[2]Department of Biological Sciences, National University of Singapore, Singapore 117543, Singapore
[3]These authors contributed equally
[4]Lead contact
*Correspondence: fengwei@tll.org.sg
https://doi.org/10.1016/j.celrep.2021.109466

SUMMARY

The evolutionarily conserved Nrf2-Keap1 pathway is a key antioxidant response pathway that protects cells/organisms against detrimental effects of oxidative stress. Impaired Nrf2 function is associated with cancer and neurodegenerative diseases in humans. However, the function of the Nrf2-Keap1 pathway in the developing nervous systems has not been established. Here we demonstrate a cell-autonomous role of the Nrf2-Keap1 pathway, composed of CncC/Nrf2, Keap1, and MafS, in governing neuronal remodeling during *Drosophila* metamorphosis. Nrf2-Keap1 signaling is activated downstream of the steroid hormone ecdysone. Mechanistically, the Nrf2-Keap1 pathway is activated via cytoplasmic-to-nuclear translocation of CncC in an importin- and ecdysone-signaling-dependent manner. Moreover, Nrf2-Keap1 signaling regulates dendrite pruning independent of its canonical antioxidant response pathway, acting instead through proteasomal degradation. This study reveals an epistatic link between the Nrf2-Keap1 pathway and steroid hormone signaling and demonstrates an antioxidant-independent but proteasome-dependent role of the Nrf2-Keap1 pathway in neuronal remodeling.

INTRODUCTION

The nervous system is remodeled often during animal development. Formation of neuronal circuits initially involves progressive events such as neurite growth, pathfinding, and synaptogenesis. At late stages, regressive events are required to refine neuronal circuits (Luo and O'Leary, 2005; Riccomagno and Kolodkin, 2015). Pruning, one of the regressive mechanisms, eliminates exuberant branches or incorrect connections without the occurrence of neuronal death and is a critical step for proper wiring of developing circuits (Schuldiner and Yaron, 2015). Pruning occurs widely across various animal species. In mammals, many neurons in the central and peripheral nervous systems often prune their excessive axons/dendrites to establish their precise and functional connections (O'Leary and Koester, 1993; Riccomagno et al., 2012; Tapia et al., 2012). Impaired pruning has been found to result in a greater dendritic spine density in layer V pyramidal neurons of individuals with autism spectrum disorder (Tang et al., 2014). Understanding the mechanisms of developmental pruning would provide important insights into the pathogenesis of human neurological disorders (Yaron and Schuldiner, 2016).

In the holometabolous insect *Drosophila*, many larval-born neurons undergo large-scale remodeling to establish the adult-specific nervous system during metamorphosis, a transition stage from larval to adult stages (Consoulas et al., 2000; Kanamori et al., 2015; Truman, 1990; Yu and Schuldiner, 2014). In the central nervous system (CNS), mushroom body (MB) γ neurons prune away their dorsal and medial axon branches as well as all dendrites and subsequently regrow the medial branches to form adult-specific circuits (Lee et al., 1999). In the peripheral nervous system (PNS), a subset of dendritic arborization (da) sensory neurons, including class I (ddaD/ddaE) and class IV (C4 da or ddaC) da neurons, prune all of their larval dendrite branches and retain their intact axons (Kuo et al., 2005; Williams and Truman, 2005), whereas class II (ddaB) and class III (ddaA/ddaF) da neurons are eliminated via apoptosis (Williams and Truman, 2005). In C4 da or ddaC neurons, dendritic blebbing and thinning initially take place at proximal regions, followed by severing or physical detachment of proximal dendrites around 6 h after puparium formation (APF), rapid fragmentation around 12 h APF, and dendritic debris clearance by 16 h APF (Figure 1A; Kuo et al., 2005; Williams and Truman, 2005). C4 da and ddaC neurons have been established as major *in vivo* models to unravel molecular and cellular mechanisms of developmental pruning in *Drosophila*. However, because of no synaptic input in sensory neurons in the PNS, dendrite pruning in ddaC mechanosensory neurons might differ from that in MB γ or other remodeling neurons in the CNS.

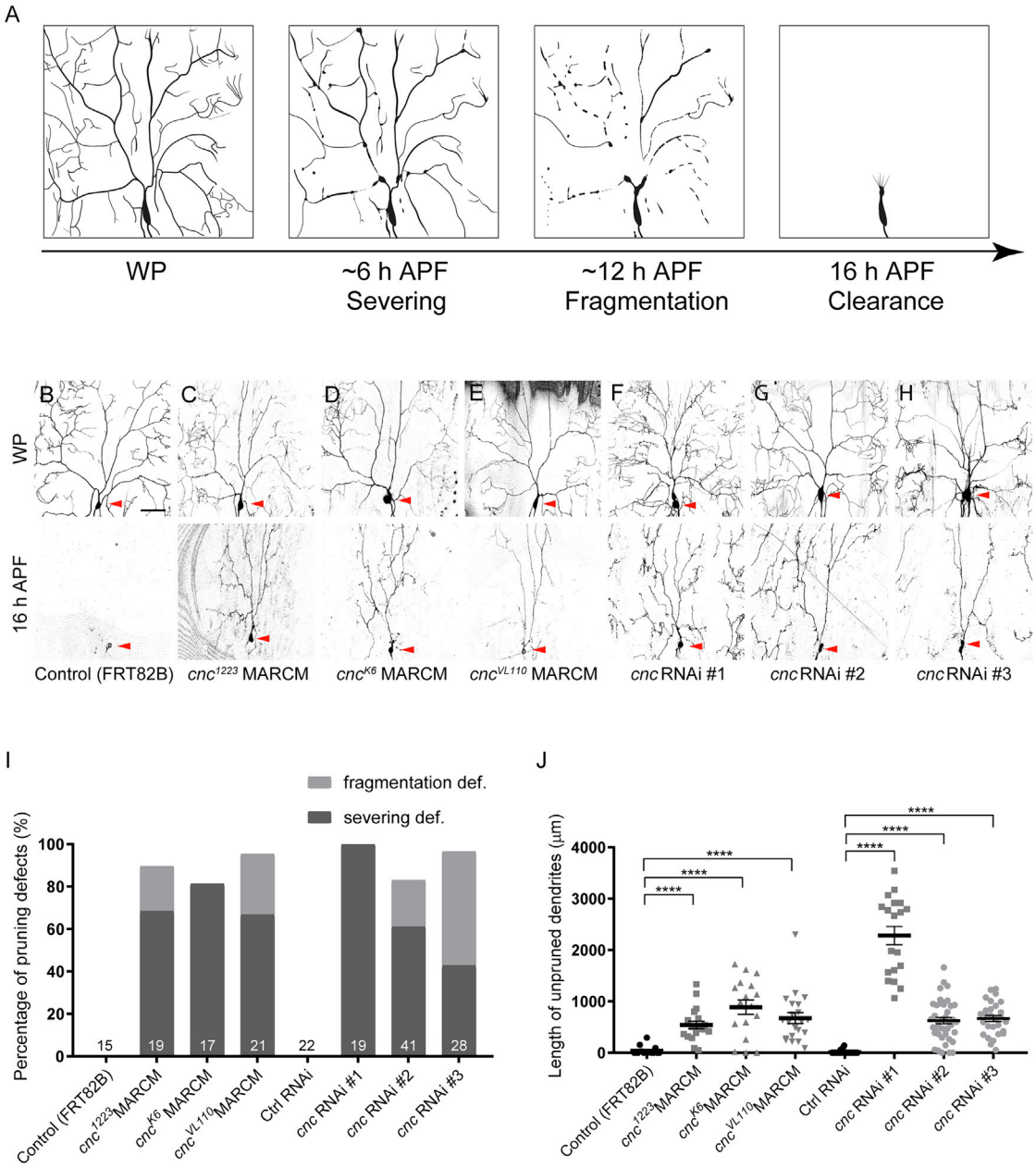

Figure 1. CncC is required cell autonomously for dendrite pruning in ddaC neurons

(A) A schematic of dendrite pruning in ddaC sensory neurons.

(B–H) Dendrites of wild-type (B), *cnc*^{1223} (C), *cnc*^{K6} (D), *cnc*^{VL110} (E), *cnc* RNAi #1 (F), #2 (G), and #3 (H) ddaC neurons at the WP and 16 h APF stages. Red arrowheads point to ddaC somata.

(I) Percentages of ddaC neurons showing pruning defects at 16 h APF.

(J) Quantitative analysis of unpruned dendrite length at 16 h APF.

Error bars represent ± SEM. The scale bar in (B) represents 50 μm. ****$p < 0.0001$. See also Figure S1.

In response to a late larval pulse of 20-hydroxyecdysone (ecdysone), ddaC neurons initiate dendrite-specific pruning by severing proximal dendrites as early as 4 h APF (Yu and Schuldiner, 2014). Ecdysone, a major insect steroid hormone, binds to a heterodimeric nuclear receptor complex comprised of the ecdysone receptor (EcR) and ultraspiracle (Usp) and induces transcriptional activation of a network of ecdysone early response genes (Thummel, 1996). In remodeling neurons, expression of the neuronal isoform EcR-B1 increases steadily from the early third-instar larval (eL3) stage, reaches its peak at the wandering third-instar larval (wL3) stage, and persists at the white prepupal (WP) stage (Kirilly et al., 2009; Kuo et al., 2005;

Lee et al., 2000), which depends on transforming growth factor β (TGF-β) signaling (Yu et al., 2013; Zheng et al., 2003), the cohesin complex (Schuldiner et al., 2008), the Ftz-F1/Hr39 nuclear receptors (Boulanger et al., 2011), and the BTB (Broad-Complex, Tramtrack and Bric-à-brac)-zinc-finger transcription factor Chinmo (Alyagor et al., 2018; Marchetti and Tavosanis, 2017). Downstream of the EcR-Usp heterodimer, the target genes are temporally induced via coordinated action between EcR-B1 and two chromatin remodelers, Brahma and CREB (cyclic AMP response element binding protein)-binding protein (Kirilly et al., 2011). At the WP stage, EcR-B1 and Usp are required to induce expression of the conserved transcription factor Sox14 and a cytosolic protein, Headcase, with unknown functions (Kirilly et al., 2009; Loncle and Williams, 2012). Sox14, in turn, promotes expression of its target genes, including the F-actin disassembly factor Mical and the ubiquitin-proteasome regulators Uba1 and Cullin-1 to promote dendrite pruning of ddaC neurons (Kirilly et al., 2009; Wong et al., 2013). Ecdysone signaling is also required to induce onset of compartmentalized calcium transients and endo-lysosomal degradation of the L1-type cell adhesion molecule Neuroglian in dendrite pruning (Kanamori et al., 2013; Zhang et al., 2014). However, whether and how ecdysone signaling regulates stress response pathways in neuronal remodeling has remained largely unknown.

In a clonal screen, we identified a basic leucine zipper (bZIP) domain-containing transcription factor, cap 'n' collar isoform C (CncC), as a player of dendrite pruning in ddaC sensory neurons. In *Drosophila*, there are at least three major Cnc isoforms: CncA, CncB, and CncC (McGinnis et al., 1998). CncC is the only isoform that shares highly conserved domains and functional relevance with its mammalian homolog nuclear factor erythroid 2-related factor 2 (Nrf2) (Kobayashi et al., 2002; Sykiotis and Bohmann, 2008). Nrf2 is a key transcriptional activator of the Nrf2-Keap1 antioxidant response pathway that maintains cellular redox homeostasis (Figure S1A). Under normal conditions, Keap1 functions as an E3 ligase adaptor to retain Nrf2 in the cytoplasm and/or promote Nrf2 degradation by the 26S proteasome (Figure S1A; Itoh et al., 1999; Motohashi and Yamamoto, 2004). Under oxidative stress conditions, Nrf2 disassociates from Keap1 and translocates to the nucleus, where it heterodimerizes with a small Maf (musculoaponeurotic fibrosarcoma) protein (Itoh et al., 1999; Zhang and Hannink, 2003). The Nrf2-Maf complex subsequently binds to antioxidant response elements (AREs) to promote expression of various detoxifying and antioxidant enzymes against oxidative stress (Figure S1A; Hayes and Dinkova-Kostova, 2014; Hochmuth et al., 2011; Motohashi and Yamamoto, 2004). In *Drosophila* and *C. elegans*, Nrf2 orthologs also enhances oxidative stress tolerance, extends the lifespan, and promotes stem cell homeostasis during aging (Bishop and Guarente, 2007; Hochmuth et al., 2011; Rodriguez-Fernandez et al., 2019; Sykiotis and Bohmann, 2008). However, despite its important functions against oxidative stress in the contexts of aging and disease, a potential role of the Nrf2-Keap1 pathway in the developing nervous systems has not been established. Here we report that the conserved Nrf2-Keap1 pathway plays a crucial role in dendrite pruning of ddaC neurons during *Drosophila* metamorphosis.

RESULTS

Cnc is required cell autonomously for dendrite pruning in ddaC neurons

In a large-scale clonal screen on 3R chromosomes (Tang et al., 2020; Wang et al., 2018), we isolated a mutant line, *l(3)1223*, that displayed the dendrite pruning defects in the majority of ddaC clones by 16 h APF (Figures 1C, 1I, and 1J). In contrast, wild-type ddaC clones completely pruned their larval dendrites (Figures 1B, 1I, and 1J). The *l(3)1223* mutant was narrowed down to the cytological region 94E4-E7 (Figure S1B). Moreover, the *l(3)1223* allele failed to complement two previously published *cnc* mutants, cnc^{K6} and cnc^{VL110} (Veraksa et al., 2000). The sequencing analysis revealed that *l(3)1223* contains a nonsense mutation in the specific coding region of the *cncC* isoform and likely results in a truncated CncC protein (amino acids 1–199) (Figure S1C), suggesting that CncC, but not CncA or CncB, is linked to the dendrite pruning defects in the *l(3)1223* allele. CncC belongs to a conserved family of bZIP domain-containing transcription factors and is the sole *Drosophila* ortholog of mammalian Nrf2 (Figure S1C). Therefore, we named *l(3)1223* as cnc^{1223} allele thereafter.

To verify that Cnc is required for dendrite pruning, we conducted a clonal analysis of cnc^{K6} and cnc^{VL110}. cnc^{K6} harbors a nonsense mutation at Q471 in the CncC-specific isoform (Veraksa et al., 2000), whereas cnc^{VL110} carries a deletion uncovering the common *cnc* region (Figure S1C; Mohler et al., 1995). Similar to cnc^{1223} clones, cnc^{K6} or cnc^{VL110} clones displayed consistent pruning defects 16 h APF (Figures 1D, 1E, 1I, and 1J). Using the class IV da neuron driver *ppk-Gal4* (Grueber et al., 2003), three independent RNAi lines (*cnc* RNAi #1, #2, and #3) led to similar dendrite pruning defects (Figures 1F–1J). The stronger pruning defect in *cnc* RNAi neurons (#1) is likely due to efficient elimination of maternal and zygotic RNA because CncC has been reported to have abundant maternal RNA deposits in early embryos (McGinnis et al., 1998). *cnc* plays an important and cell-autonomous role in regulating dendrite pruning in ddaC sensory neurons.

The C isoform CncC promotes dendrite pruning via its bZIP DNA-binding domain

Three major Cnc isoforms, CncA, CncB, and CncC, share a common bZIP DNA-binding and dimerization domain at their carboxy-terminal (C-terminal) regions, with CncC being the largest one (Figure 2A; McGinnis et al., 1998). CncC also contains the unique DLG and ETGE motifs, two conserved binding sites for its negative regulator Keap1, at its amino-terminal (N-terminal) region (Figure 2A). To ascertain whether CncC is the isoform required for dendrite pruning, we conducted rescue experiments using the individual isoforms. Indeed, overexpression of CncC, but not CncA or CncB, was able to fully rescue the pruning defects in cnc^{1223} mutant neurons (Figures 2C–2E, 2J, and 2K). As controls, overexpression of these Cnc isoforms alone did not affect normal dendrite pruning (Figure S2A). Thus, these rescue results demonstrate that CncC is critical for dendrite pruning in ddaC neurons.

Interestingly, by using an anti-Cnc antibody against the common region (P4) (Figure S1C), we observed cytoplasmic

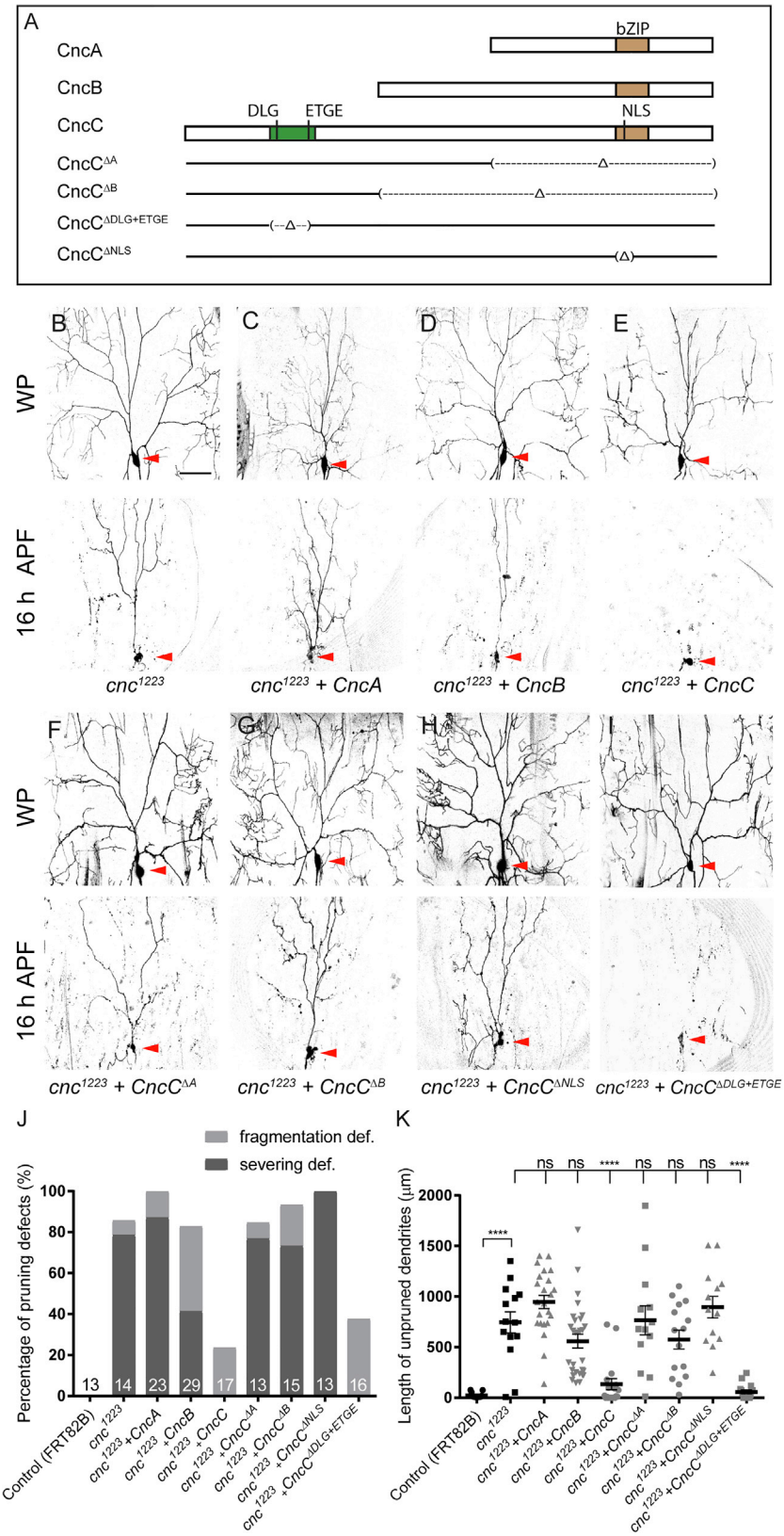

Figure 2. The C isoform CncC promotes dendrite pruning via its bZIP DNA-binding domain

(A) A schematic showing the full-length CncA, CncB, and CncC proteins with different domains as well as various truncated CncC proteins.

(B–I) Dendrites of cnc^{1223} (B), cnc^{1223} + *CncA* (C), cnc^{1223} + *CncB* (D), cnc^{1223} + *CncC* (E), cnc^{1223} + $CncC^{\Delta A}$ (F), cnc^{1223} + $CncC^{\Delta B}$ (G), cnc^{1223} + $CncC^{\Delta NLS}$ (H), and cnc^{1223} + $CncC^{\Delta DLG+ETGE}$ (I) ddaC neurons at the WP and 16 h APF stages. Red arrowheads point to ddaC somata.

(J) Percentages of ddaC neurons showing pruning defects at 16 h APF.

(K) Quantitative analysis of unpruned dendrite length at 16 h APF.

Error bars represent ± SEM. The scale bar in (B) represents 50 μm. ns, not significant; ****$p < 0.0001$. See also Figure S2.

localization of overexpressed CncC at the wL3 stage, in contrast to nuclear enrichment of CncA or CncB (Figure S2B). To understand the mechanism of CncC action, we first performed a structure-function analysis by generating a series of CncC deletions (Figure 2A). Overexpression of either of two C-terminal deletions, CncC$^{\Delta A}$ and CncC$^{\Delta B}$, failed to rescue the pruning defects in *cnc*^{1223} mutant clones (Figures 2F, 2G, 2J, and 2K), suggesting that the bZIP domain is required for CncC function during dendrite pruning. Importantly, overexpression of CncC$^{\Delta NLS}$, which removes its nuclear localization sequence (NLS) and the DNA-binding ability within the bZIP domain (Veraksa et al., 2000), was unable to rescue the pruning defects observed in *cnc*^{1223} mutant clones (Figures 2H, 2J, and 2K). These data suggest that, despite its cytoplasmic distribution (Figure S2B), CncC likely functions as a transcription factor during dendrite pruning. In addition, overexpression of the CncC$^{\Delta DLG+ETGE}$ truncate lacking the Keap1-binding sites led to complete rescue in the severing defects of *cnc*^{1223} mutant clones (Figures 2I, 2J, and 2K). As controls, overexpression of these CncC truncates alone did not impair the normal dendrite pruning process (Figure S2A). Thus, CncC probably acts as a transcription factor to induce its downstream gene expression during dendrite pruning.

The conserved Nrf2-Keap1 pathway is critical for dendrite pruning in ddaC neurons

There is a sole *Drosophila* ortholog of the small Maf, MafS, which functions as an Nrf2 transcriptional coactivator (Figure S1A; Veraksa et al., 2000). Given that no *mafS* mutant was available, we took advantage of the CRISPR-Cas9 technology to generate two insertion or deletion (indel) mutants, *mafS*$^{9-1}$ and *mafS*$^{8-3}$ (Figure 3A). Importantly, MARCM clones generated from *mafS*$^{9-1}$ or *mafS*$^{8-3}$ mutant exhibited consistent dendrite pruning defects at 16 h APF (Figures 3C, 3D, 3L, and 3M), similar to *cnc*^{1223} clones (Figures 1C, 1I, and 1J), in contrast to wild-type clones (Figures 3B, 3L, and 3M). Overexpression of hemagglutinin (HA)-tagged MafS (MafS-HA) in *mafS*$^{9-1}$ or *mafS*$^{8-3}$ MARCM mutant clones was able to completely rescue their respective pruning defects (Figures 3E, 3F, 3L, and 3M), confirming that these dendrite pruning phenotypes are caused by loss of *mafS* function. Overexpressed MafS-HA was localized in the nuclei (Figure S3A) and did not disturb the normal progression of dendrite pruning (Figure S3B).

We next interrogated the involvement of the repressor Keap1 in dendrite pruning. If Keap1 antagonizes CncC activity, then one would expect that Keap1 overexpression phenocopies loss of *cncC* function. Indeed, Keap1 overexpression led to the dendrite pruning defects in most ddaC neurons at 16 h APF (Figures 3H, 3L, and 3M), similar to loss of *cncC* function (Figures 1C, 1I, and 1J; wild-type, see Figures 3G, 3L, and 3M). To further support their antagonism, we overexpressed Keap1 in *cnc*^{1223} MARCM mutant clones and compared it with *cnc*^{1223} mutant clones or wild-type clones overexpressing Keap1. All *cnc*^{1223} mutant ddaC neurons overexpressing Keap1 exhibited much stronger severing defects with full penetrance, in contrast to 43% in *cnc*^{1223} clones and 10% in Keap1-overexpressing neurons (via a single copy of *ppk-Gal4*) (Figures 3I–3K, 3L, and 3M). In addition, neither CncC overexpression nor loss of *keap1* function led to precocious dendrite pruning at 6 h APF or impaired dendrite pruning at 16 h APF (Figure S3C).

The evolutionarily conserved Nrf2-Keap1 pathway probably regulates dendrite pruning via transcriptional activation of its downstream targets.

The Nrf2-Keap1 pathway is activated by ecdysone signaling prior to dendrite pruning

We next investigated the relationship between the Nrf2-Keap1 pathway and ecdysone signaling. EcR-B1 and Mical expressions were upregulated in wild-type ddaC neurons at the WP stage (Figure S2C; Kirilly et al., 2009). However, their expression was not impaired in *cncC* mutants or RNAi ddaC neurons (Figure S2C). Similarly, Keap1 overexpression or loss of *keap1* function did not impair upregulation of EcR-B1 and Mical expression in ddaC neurons (Figure S2C). Thus, these data suggest that the Nrf2-Keap1 pathway is not required to induce ecdysone signaling during neuronal remodeling. This result contrasts a recent report showing that CncC and Keap1 cooperatively activate ecdysone signaling in salivary glands (Deng and Kerppola, 2014).

We next attempted to determine whether the Nrf2-Keap1 pathway is activated by ecdysone signaling. *gstD1-lacZ* reporter represents endogenous expression of the detoxifying gene *gstD1*, a *bona fide* target gene of CncC, because β-galactosidase is expressed under control of a *gstD1* regulatory sequence (Hochmuth et al., 2011; Sykiotis and Bohmann, 2008). We therefore assessed whether *gstD1-lacZ* is also a reliable reporter detecting activation of the Nrf2-Keap1 pathway in ddaC neurons. Interestingly, although *gstD1-lacZ* was undetectable from the wL3 to WP stages (Figure 4A), it exhibited a significant increase in ddaC neurons at 6 APF (Figure 4A), a stage before onset of dendrite pruning. Importantly, RNAi knockdown of *cnc* via two RNAi lines (#1 and #2) significantly reduced *gstD1-lacZ* expression at 6 h APF (Figure 4B). Consistent with its role as a CncC inhibitor, Keap1 overexpression significantly suppressed *gstD1-lacZ* expression at 6 h APF (Figure 4C). Conversely, when CncC was overexpressed in ddaC neurons, *gstD1-lacZ* expression was augmented significantly at 6 h APF (Figure 4C). Although CncC was overexpressed continuously by the *ppk-Gal4* driver from the late embryonic stages to the pupal stages, the *gstD1-lacZ* reporter was only induced as early as 3 h APF (Figure S4A). As a control, CncA overexpression did not augment *gstD1-lacZ* expression at 6 h APF (Figure S4B). Similar to CncC overexpression, knockdown of *keap1* via two independent RNAi lines (#1 and #2) led to significant increases in *gstD1-lacZ* levels in ddaC neurons (Figure 4D). These *gstD1-lacZ* results demonstrate that the Nrf2-Keap1 pathway is activated prior to dendrite pruning.

We next attempted to investigate whether ecdysone signaling is responsible for activation of Nrf2-Keap1 pathway. When ecdysone signaling is inhibited via the dominant-negative form of EcR (EcR^{DN}) or RNAi knockdown of its co-receptor Usp, *gstD1-lacZ* expression was almost completely abolished in ddaC neurons at 6 h APF (Figures 4E and 4F). Likewise, RNAi knockdown of their downstream transcription factor Sox14 also eliminated *gstD1-lacZ* expression at the same time point (Figure 4F). In

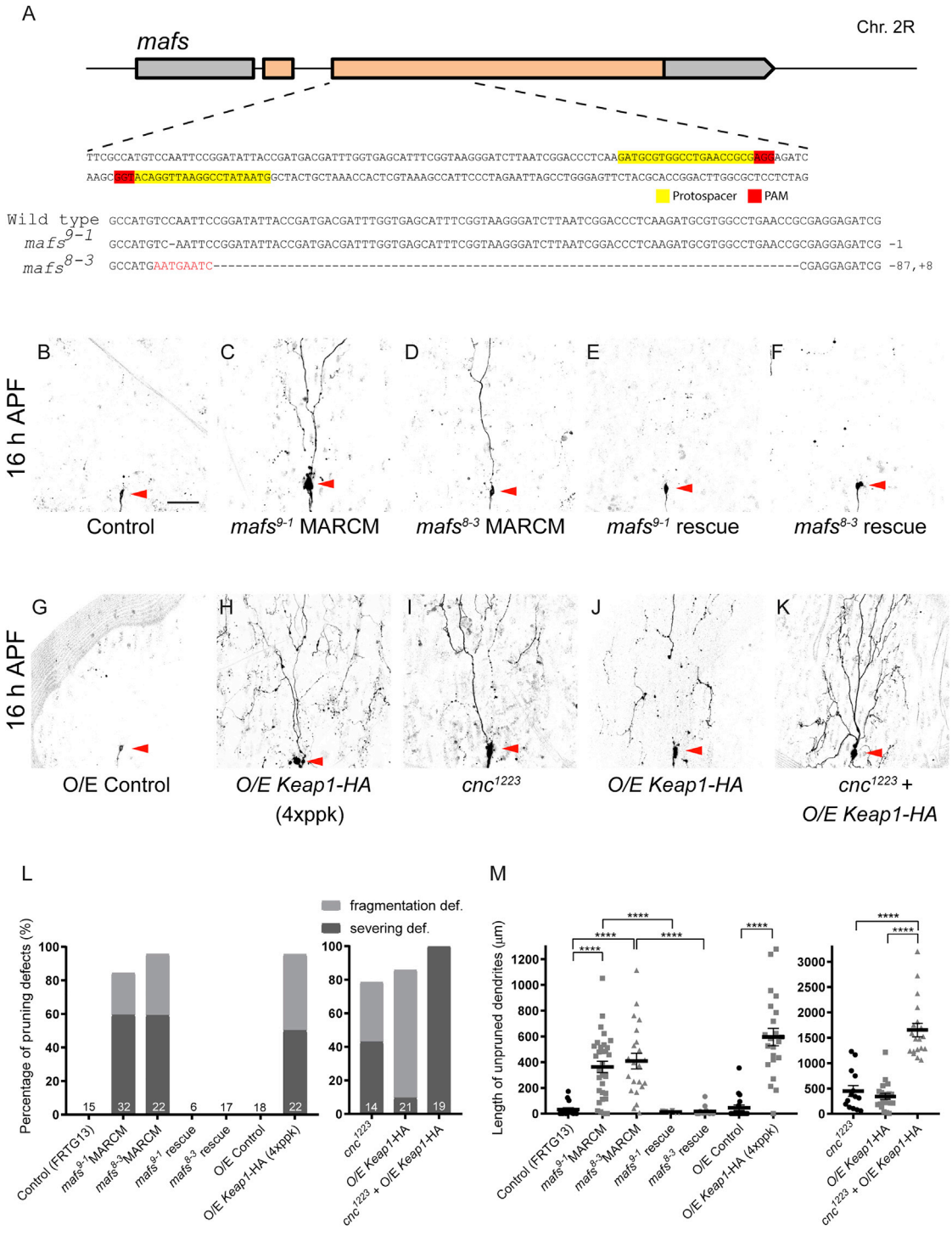

Figure 3. The conserved Nrf2-Keap1 pathway governs dendrite pruning in ddaC neurons

(A) A schematic of the gene structure of *mafs* and two mutant alleles, $mafs^{9-1}$ and $mafs^{8-3}$.

(B–K) Dendrites of wild-type (B), $mafs^{9-1}$ (C), $mafs^{8-3}$ (D), $mafs^{9-1}$ rescue (E), $mafs^{8-3}$ rescue (F), control overexpression (G), Keap1-HA overexpression (H), cnc^{1223} (I), Keap1-HA overexpression (J), and cnc^{1223} with Keap1-HA overexpression (K) ddaC neurons at 16 h APF. Red arrowheads point to ddaC somata.

(L) Percentages of ddaC neurons showing pruning defects at 16 h APF.

(M) Quantitative analysis of unpruned dendrite length at 16 h APF.

Error bars represent ± SEM. The scale bar in (B) represents 50 μm. ****$p < 0.0001$. See also Figure S3.

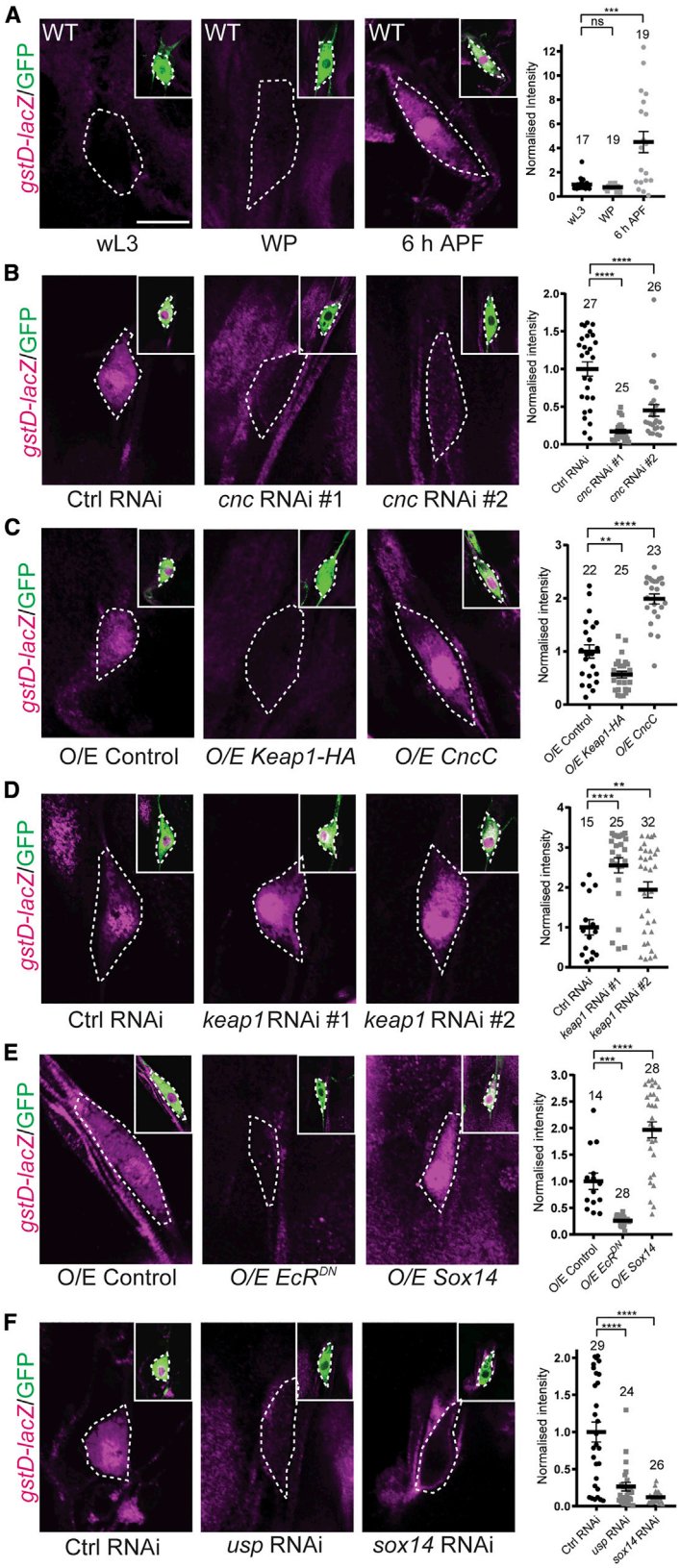

Figure 4. The Nrf2-Keap1 pathway is activated by ecdysone signaling prior to dendrite pruning

(A) Expression of *gstD-lacZ* in wild-type ddaC neurons at the wL3, WP, and 6 h APF stages.

(B–F) Expression of *gstD-lacZ* in control RNAi and *cnc* RNAi #1 and #2 (B); control and Keap1-HA and CncC overexpression (C); control RNAi and *keap1* RNAi #1 and #2 (D); control and EcR^{DN} and Sox14 overexpression (E); and control RNAi, *usp* RNAi, and *sox14* RNAi (F) ddaC neurons at 6 h APF.

ddaC somata are marked by dashed lines. Quantitative analyses of normalized *gstD1*-lacZ fluorescence are shown in the right panels. Error bars represent ± SEM. The scale bar in (A) represents 10 μm. ns, not significant, $^{**}p < 0.01$, $^{***}p < 0.001$, $^{****}p < 0.0001$. See also Figure S4.

contrast, the F-actin disassembly regulator Mical is not required for activation of the Nrf2-Keap1 pathway in ddaC neurons (Figure S4C). To examine whether forced activation of ecdysone signaling is sufficient to induce nuclear accumulation of CncC protein at earlier time points, we overexpressed Sox14, which has been shown to precociously induce Mical expression and dendrite pruning (Kirilly et al., 2009). Strikingly, Sox14 overexpression caused a significant increase in *gstD1-lacZ* levels in ddaC neurons at 6 h APF (Figure 4E). Ecdysone signaling is necessary and sufficient to induce activation of the Nrf2-Keap1 pathway before onset of dendrite pruning.

CncC is translocated from the cytoplasm to the nucleus, depending on importin and ecdysone signaling

We next attempted to understand the mechanism of how ecdysone signaling activates the Nrf2-Keap1 pathway during dendrite pruning. We found that overexpressed CncC was localized in the cytoplasm of ddaC neurons at the wL3 stage (Figure S2B); however, its DNA-binding bZIP domain is required for dendrite pruning (Figure 2H). These data suggest that CncC might translocate from the cytoplasm to the nucleus in ddaC neurons in response to the steroid hormone ecdysone and function as a transcription factor to activate its downstream gene expression. Given that no functional antibody is available for detecting endogenous CncC protein in sensory neurons, we first made a huge effort to generate various antibodies against four regions of the protein. Among them, a functional antibody against the CncC-specific epitope (P2) was isolated (Figure S1C). This antibody is specific for CncC because immunofluorescence signals seen in wild-type ddaC neurons were largely eliminated in *cnc* RNAi neurons (Figure S5A) but increased strongly upon CncC overexpression (Figure S5B). Importantly, we indeed observed its cytoplasmic-to-nuclear translocation of the endogenous CncC protein during the larval-to-pupal transition. In the wild type, the endogenous CncC protein was mainly localized in the cytoplasm of ddaC neurons at the wL3 stage (Figure 5A), similar to the overexpressed protein (Figure S5B, low exposure; see also Figure S2B). At the WP stage, endogenous CncC protein began to exhibit weak accumulation in the nuclei (Figure 5A). The intensity of nuclear CncC levels was elevated significantly in ddaC neurons at 6 and 8 h APF (Figure 5A), suggesting a cytoplasmic-to-nuclear translocation of endogenous CncC protein. Consistent with its role as a CncC inhibitor, knockdown of *keap1* (#1) led to a significant increase in nuclear CncC levels in ddaC neurons at 6 h APF (Figure 5B). Conversely, Keap1 overexpression led to a significant reduction in nuclear CncC expression levels at 6 h or 8 h APF (Figures 5B and S5C). The importin complex is required to mediate protein translocation from the cytoplasm into the nucleus (Otis et al., 2006). To further substantiate the cytoplasmic-to-nuclear translocation of CncC, we abolished the importin complex by knocking down the sole fly Importin-β (Imp-β) subunit. Interestingly, knockdown of Imp-β largely abolished CncC nuclear accumulation because the majority of CncC protein was present in the cytoplasm at 8 h APF (Figure 5C). Knockdown of Imp-β also led to severe dendrite pruning defects in all ddaC neurons (Figure S5D). These data indicate cytoplasmic-to-nuclear translocation of endogenous CncC protein in *Drosophila*.

We then investigated whether ecdysone signaling is responsible for cytoplasmic-to-nuclear translocation of CncC. Interestingly, RNAi knockdown of EcR, Usp, or Sox14 led to a strong reduction in nuclear CncC expression in ddaC neurons at 6 h APF (Figure 5C) and the WP stage (Figure S5E). Strikingly, Sox14 overexpression caused significant increases in nuclear CncC levels as early as the wL3 and WP stages (Figure 5D). In contrast, *mical* RNAi knockdown did not affect normal nuclear CncC levels at 6 h APF (Figure S5F). Vice versa, CncC is not required for Mical upregulation either (Figure S2C). Our data suggest that CncC acts downstream of Sox14 but in parallel to Mical during dendrite pruning.

Our data demonstrate that ecdysone signaling is necessary and sufficient to facilitate cytoplasmic-to-nuclear translocation of CncC before dendrite pruning. Moreover, nuclear CncC is required to activate the Nrf2-Keap1 pathway and promote dendrite pruning during early metamorphosis.

CncC regulates dendrite pruning independent of its antioxidant function

To understand whether the Nrf2-Keap1 pathway regulates dendrite pruning via its downstream antioxidant response pathway (Figure S1A), we systematically interrogated the roles of antioxidant enzymes in dendrite pruning. First we investigated whether overexpression of the downstream antioxidant enzymes suppresses *cnc* RNAi or mutant phenotypes. Sod and catalase are well-characterized antioxidant enzymes that act together to remove reactive oxygen species in *Drosophila* stem cells or neurons (Liu et al., 2015; Milton et al., 2011; Owusu-Ansah and Banerjee, 2009). Overexpression of Sod1, Sod2, hSod1, or catalase was not able to rescue or suppress the dendrite pruning defects in *cnc* RNAi neurons (Figures 6B–6E, 6K, and 6L) or cnc^{1223} mutant clones (Figures 6H, 6K, and 6L), similar to their respective controls (Figures 6A, 6G, 6K, and 6L). Glutamate-cysteine ligase catalytic/modifier subunits (Gclc/Gclm) are the rate-limiting enzymes for glutathione biosynthesis, reducing the intracellular redox state in flies (Orr et al., 2005), whereas Jafrac1 is a key thioredoxin peroxidase that protects cells from oxidative stress (Radyuk et al., 2003). Gclm, Gclc, and Jafrac1 are antioxidant targets of the Nrf2-Keap1 pathway in flies and mammals (Hayes and Dinkova-Kostova, 2014; Hochmuth et al., 2011; Wang et al., 2015). Their overexpression was able to rescue the *cncC* mutant defects in fly intestine stem cells (Hochmuth et al., 2011). However, like Sod1/2 and catalase, Jafrac1, Gclc, or Gclm overexpression did not rescue the dendrite pruning defects in *cnc* RNAi (Figures 6F, 6K, and 6L) or cnc^{1223} neurons (Figures 6I–6L). In addition, gain or loss of these antioxidant enzymes did not disturb normal progression of dendrite pruning (Figures S6A and S6B). Thus, CncC-mediated dendrite pruning does not require activation of these downstream antioxidant enzymes.

We further ruled out the possibility that the dendrite pruning defects in *cnc* neurons are caused by elevated oxidative stress. Mitochondria are major organelles that generate most reactive oxygen species and, therefore, oxidative stress during cellular metabolism. Mitochondrial dysfunction leads to high oxidative stress and age-dependent neurodegeneration in *Drosophila* and mammals (Liu et al., 2015). We directly disrupted normal mitochondrial metabolism and examined whether mitochondrial dysfunction impairs dendrite pruning in ddaC neurons. Knockdown of ND42 or

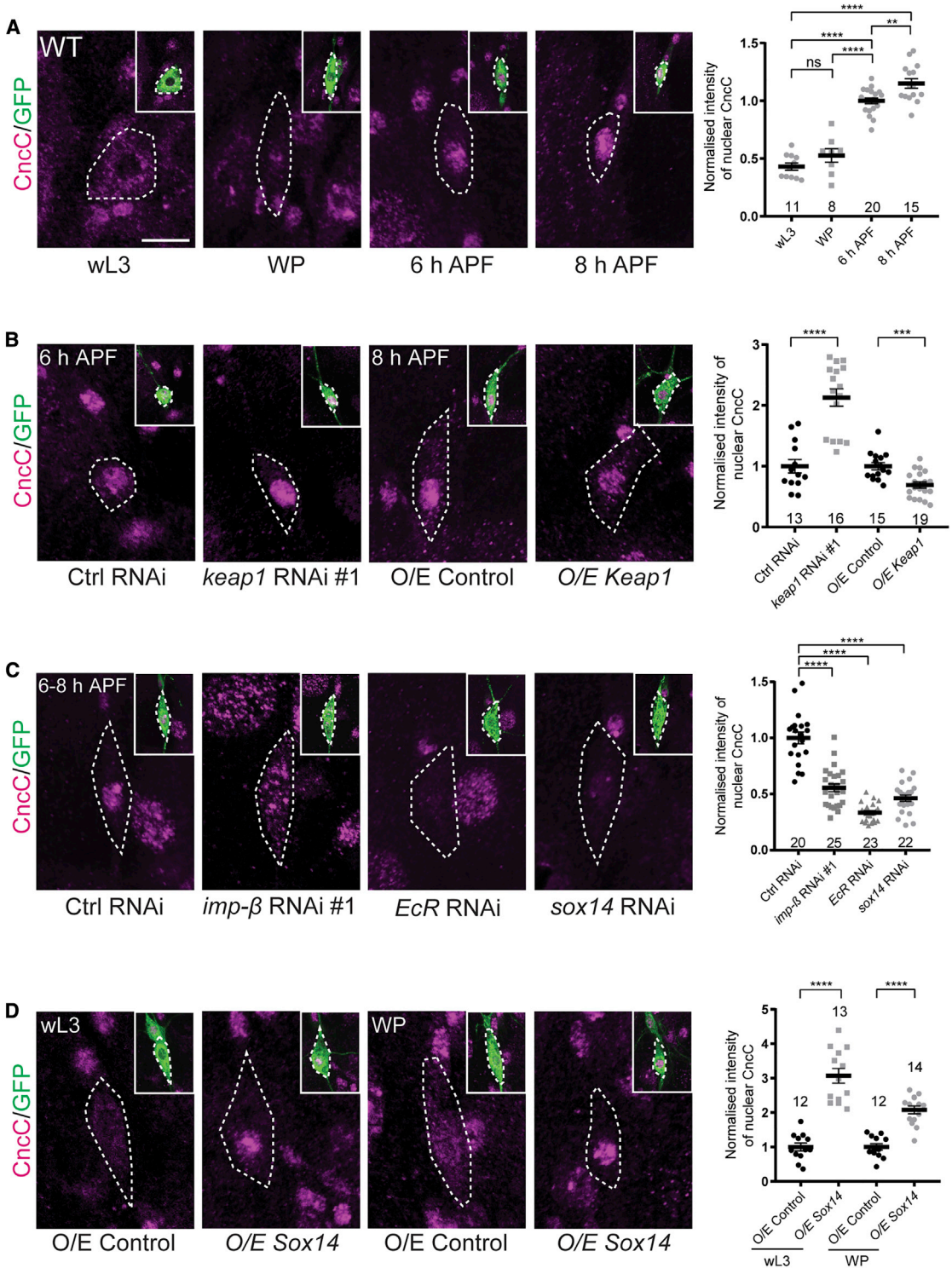

Figure 5. CncC is translocated from the cytoplasm to the nucleus in an importin- and ecdysone-signaling-dependent manner

(A) Expression of CncC in wild-type ddaC neurons at the wL3, WP, 6 h APF, and 8 h APF stages.

(B–D) Expression of CncC in ddaC neurons with control RNAi, *keap1* RNAi #1, and control and Keap1 overexpression at 6 or 8 h APF (B); control RNAi, *imp-β* RNAi #1, *EcR* RNAi, and *sox14* RNAi at 6–8 h APF (C); and control and Sox14 overexpression at the wL3 and WP stages (D). ddaC somata are marked by dashed lines. Quantitative analyses of normalized nuclear CncC fluorescence are shown in the right panels.

Error bars represent ± SEM. The scale bar in (A) represents 10 μm. ns, not significant, $^{**}p < 0.01$, $^{***}p < 0.001$, $^{****}p < 0.0001$. See also Figure S5.

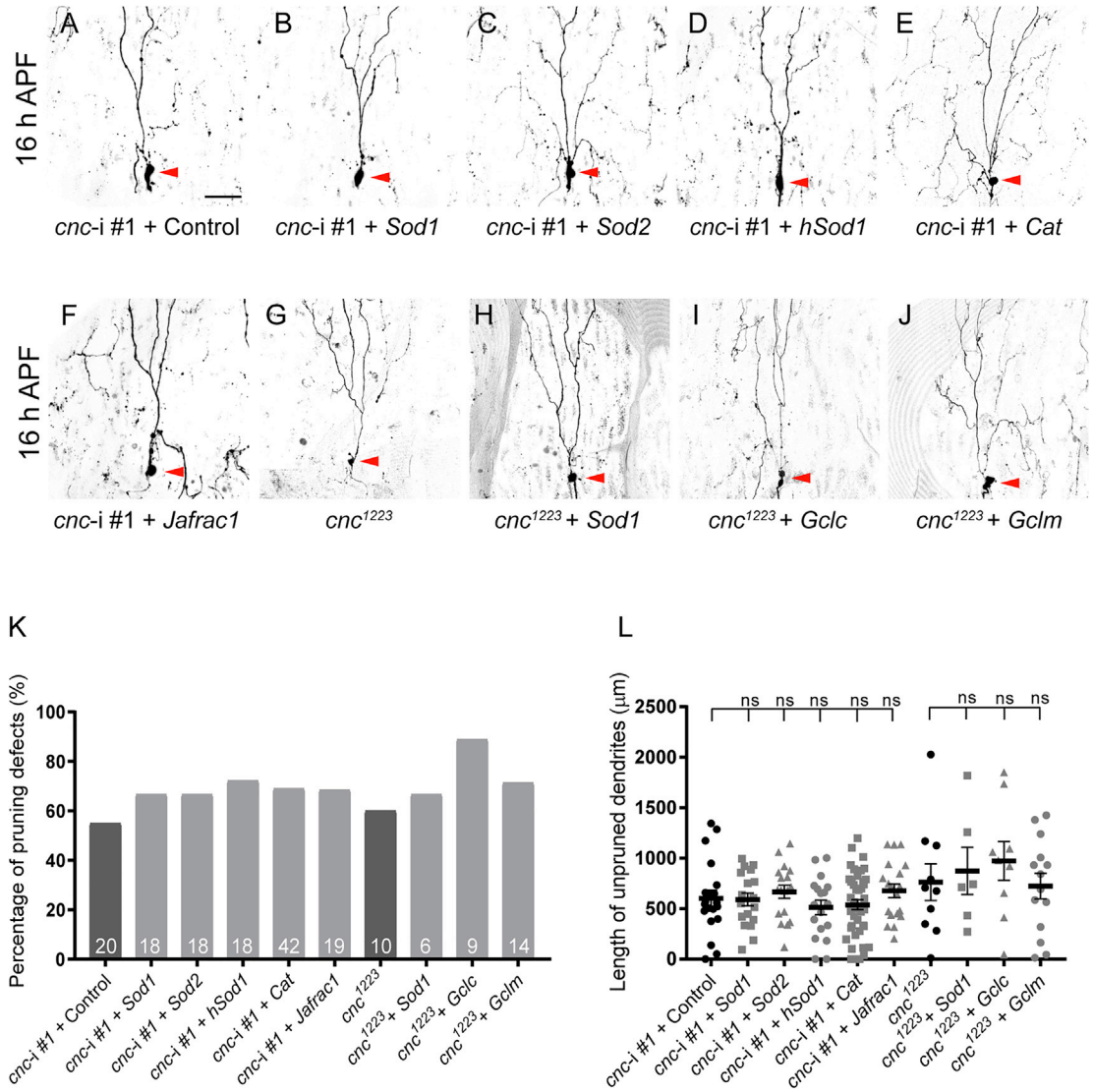

Figure 6. CncC regulates dendrite pruning independent of its antioxidant function

(A–F) Dendrites of *cnc* RNAi #1 ddaC neurons with control (A), Sod1 (B), Sod2 (C), hSod1 (D), catalase (E), and Jafrac1 (F) overexpression at 16 h APF.

(G–J) Dendrites of cnc^{1223} ddaC clones (G) with Sod1 (H), Gclc (I), and Gclm (J) overexpression at 16 h APF. Red arrowheads point to ddaC somata.

(K) Percentages of ddaC neurons showing pruning defects at 16 h APF.

(L) Quantitative analysis of unpruned dendrite length at 16 h APF.

Error bars represent ± SEM. The scale bar in (A) represents 50 μm. ns, not significant. See also Figure S6.

ND75, two key components of complex I of the mitochondrial electron transport chain, has been reported to significantly increase intracellular oxidative stress in neurons and stem cells (Hochmuth et al., 2011; Liu et al., 2015; Owusu-Ansah and Banerjee, 2009). RNAi knockdown of ND42 or ND75 via multiple functional RNAi constructs (Hochmuth et al., 2011; Liu et al., 2015) did not cause any dendrite pruning defect at 16 h APF (Figure S6C). Loss of *Marf* or *Aats-met* function has been shown to increase neuronal oxidative stress and cause age-dependent neurodegeneration in flies (Liu et al., 2015). However, similar to ND42 or ND75 knockdown, ddaC clones from *Aats-met* or *Marf* mutants exhibited normal dendrite pruning in ddaC neurons (Figure S6C). Thus, these data, albeit negative, suggest that high oxidative stress appears to have no effect on dendrite pruning during development, in contrast to its detrimental effect on neurodegeneration during aging reported in a previous study (Liu et al., 2015).

These data strongly suggest that CncC plays an unexpected role in regulating dendrite pruning independent of its canonical antioxidant response pathway.

The Nrf2-Keap1 pathway regulates the proteasome degradation activity in ddaC neurons

To understand how the Nrf2-Keap1 pathway governs dendrite pruning, we observed prominent accumulation of

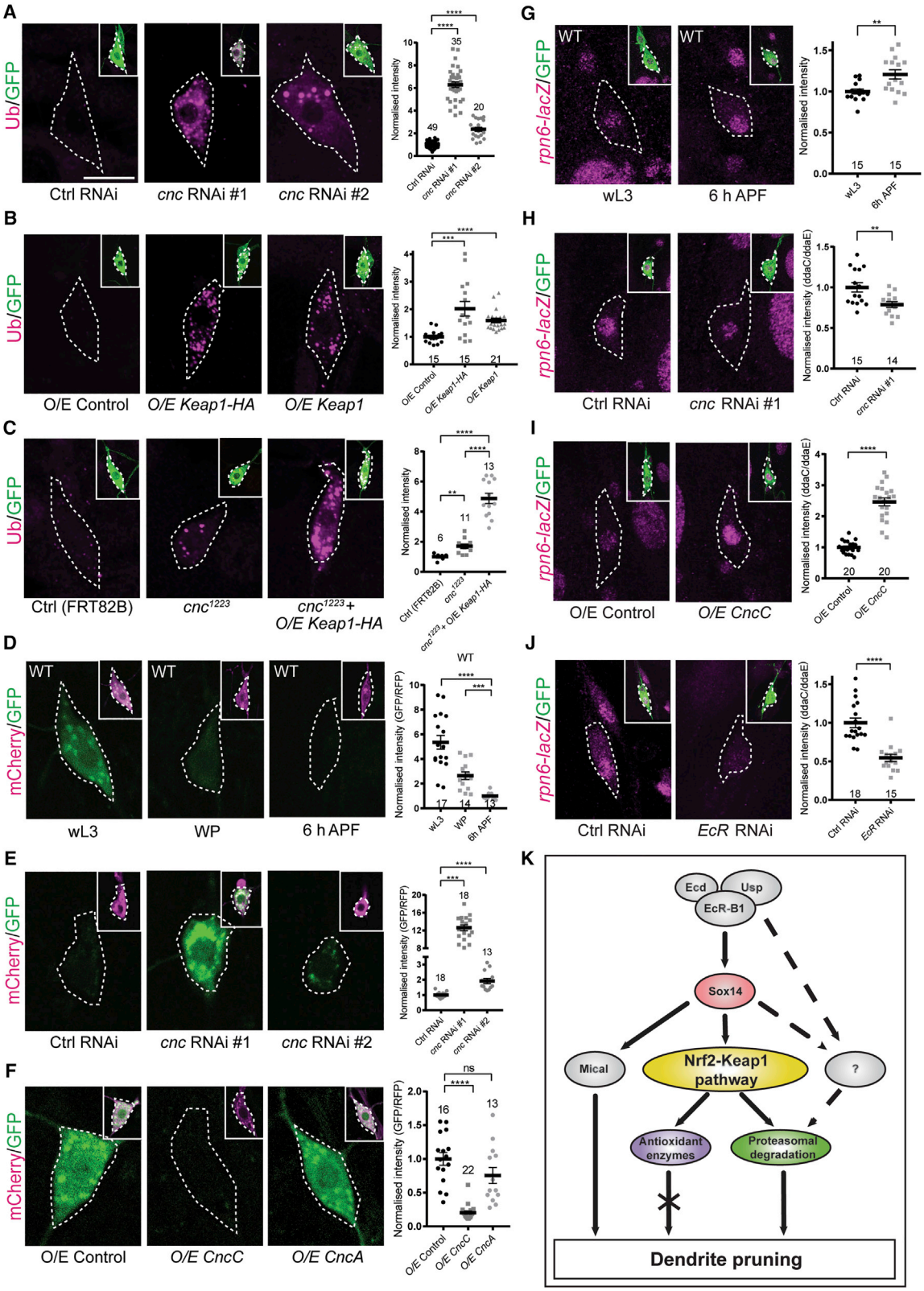

(legend on next page)

ubiquitin-positive aggregates in the somata of *cnc* RNAi (#1 and #2) (Figures 7A) or cnc^{1223} MARCM mutant ddaC neurons (Figures 7C). Likewise, overexpression of Keap1-HA or Keap1 also resulted in aggregation of poly-ubiquitinated proteins (Figures 7B) in ddaC neurons. In contrast, control ddaC neurons displayed undetectable ubiquitin aggregates in their somata (Figures 7A–7C). Compared with the cnc^{1223} mutant alone (Figure 7C), cnc^{1223} mutant ddaC neurons overexpressing Keap1 exhibited a synergistic increase in the level of ubiquitinated protein aggregates (Figure 7C) that correlated with their severe dendrite pruning defects (Figures 3K–3M). Like *cnc* RNAi or mutant neurons, $mafS^{9-1}$ mutant clones also exhibited ubiquitin-positive protein aggregates (Figure S7A). Similarly, upon knockdown of Mov34 or Rpn7, two 19S proteasomal subunits, even more robust ubiquitinated proteins accumulated and formed 2–3 enlarged structures (Figure S7A), suggesting severely impaired UPS function. Interestingly, CncC did not accumulate in those ubiquitin-positive puncta in the cytoplasm and, instead, was enriched in the nuclei of *mov34* or *rpn7* RNAi ddaC neurons (Figure S7B). These data suggest that the Nrf2-Keap1 pathway is required for proper proteasome function in ddaC neurons.

We next assessed whether the accumulation of ubiquitinated proteins in *cncC* mutant neurons is due to impaired proteasome gene expression and/or function. We performed real-time PCR experiments in *cnc* RNAi knockdown and wild-type larval brains to examine the mRNA levels of various proteasomal subunits. Importantly, we observed that CncC is required for transcription of the 20S and 19S proteasomal subunits, in contrast to the role of mammalian Nrf2 only in expressing 20S catalytic core (Kwak et al., 2003; Towers et al., 2019). The mRNA levels of Prosβ1, Prosβ2, Prosβ5, Prosα4, and Prosα7 of the 20S core particle as well as Rpn3 and Rpn11 of the 19S regulatory particle were reduced significantly in *cnc* RNAi knockdown brains compared with those in the wild-type control (Figure S7C). Our findings suggest that CncC upregulates proteasome gene expression and promotes proteasomal degradation activity in ddaC neurons. We overexpressed Prosβ5, an endopeptidase subunit of the 26S proteasome, in *cncC* RNAi ddaC neurons but observed no significant suppression of the dendrite pruning defects (Figure S7D), suggesting that overexpression of a single proteasomal subunit is not sufficient to restore proteasomal degradation activity. In addition, ubiquitinated protein aggregates in *cnc* RNAi neurons were not rescued or suppressed by overexpression of Sod1, catalase, or Jafrac1 (Figure S7E).

To further strengthen the conclusion that the poly-ubiquitinated protein accumulation is due to impaired proteasome activity, we utilized the reporter CL1-GFP, a GFP protein fused with a degradation signal to induce its proteasomal degradation (Bence et al., 2001; Pandey et al., 2007). This CL1-GFP protein is degraded rapidly by the 26S proteasome, and its steady-state levels reflect the level of proteasome activity (Pandey et al., 2007). In wild-type ddaC neurons, the levels of CL1-GFP were downregulated drastically from wL3 to WP to 6 h APF (Figure 7D), suggesting a trend of increases in proteasomal degradation activity before dendrite pruning. Knockdown of CncC (#1 and #2) led to significant increases in CL1-GFP levels in ddaC neurons at 6 h APF (Figure 7E), indicative of impaired proteasomal degradation. Importantly, overexpression of CncC, but not CncA, was able to significantly accelerate CL1-GFP degradation at wL3 (Figure 7F), a larval stage when fusion is normally stable and abundant in wild-type neurons (Figures 7D and 7F). These data further support the hypothesis that the Nrf2-Keap1 pathway is necessary and sufficient to promote proteasome-mediated protein degradation prior to dendrite pruning.

To substantiate the conclusion that CncC is required to upregulate the proteasomal degradation machinery at the onset of ddaC dendrite pruning, we screened available *lacZ* reporter lines for their expression in ddaC neurons. From this screen, we isolated a *rpn6-lacZ* reporter line ($rpn6^{K00103}$). *rpn6-lacZ* expression was upregulated in wild-type ddaC neurons from wL3 to 6 h APF (Figure 7G). Its expression was downregulated significantly in *cnc* RNAi ddaC neurons (Figure 7H). Moreover, overexpression of CncC strongly upregulated *rpn6-lacZ* expression in ddaC neurons at the wL3 and 6 h APF stages (Figures 7I and S7F). These *in vivo* data further suggest that the Nrf2-Keap1 pathway is necessary and sufficient to upregulate the expression of proteasomal subunits in ddaC neurons and enhance the proteasomal degradation machinery prior to dendrite pruning. More importantly, *rpn6-lacZ* expression also depends on EcR and Sox14 because its expression level was downregulated significantly upon EcR or Sox14 knockdown (Figures 7J and S7G). The expression levels of *rpn6-lacZ* were reduced more severely in *EcR* RNAi or *sox14* RNAi ddaC neurons compared with those in *cnc* RNAi neurons. These findings are in line with our model (Figure 7K) proposing that other, still unidentified factors/pathways might function downstream of ecdysone signaling but act

Figure 7. CncC regulates dendrite pruning by enhancing proteasome function

(A–C) Accumulation of ubiquitin-positive aggregates in ddaC neurons with control RNAi and *cnc* RNAi #1 and #2 (A); control, Keap1-HA, and Keap1 overexpression (B); and control, cnc^{1223}, and cnc^{1223} with Keap1-HA overexpression (C) at the wL3 stage. Quantitative analyses of normalized ubiquitin fluorescence are shown in the right panels.

(D) Expression of CL1-GFP proteins in wild-type ddaC neurons at the wL3, WP, and 6 h APF stages. Quantitative analysis of normalized GFP/RFP fluorescence are shown in the right panel.

(E and F) Expression of CL1-GFP proteins in ddaC neurons with control RNAi and *cnc* RNAi #1 and #2 at 6 h APF (E) and control and CncC and CncA overexpression at wL3 (F). Quantitative analyses of normalized GFP/RFP fluorescence are shown in the right panels.

(G) Expression of *rpn6-lacZ* in wild-type ddaC neurons at wL3 and 6 h APF. Quantitative analyses of normalized *rpn6-lacZ* fluorescence are shown in the right panel.

(H–J) Expression of *rpn6-lacZ* in ddaC neurons with control RNAi and *cnc* RNAi #1 (H), control and CncC overexpression (I), and control RNAi and *EcR* RNAi (J) at 6 h APF. ddaC somata are marked by dashed lines. Quantitative analyses of normalized *rpn6-lacZ* fluorescence (ddaC/ddaE) are shown in the right panels.

(K) A schematic of the proposed working model.

Error bars represent ± SEM. The scale bar in (A) represents 10 μm. ns, not significant, $^{**}p < 0.01$, $^{***}p < 0.001$, $^{****}p < 0.0001$. See also Figure S7.

in parallel to the Nrf2-Keap1 pathway to regulate the proteasomal degradation machinery during dendrite pruning.

DISCUSSION

A critical role of the Nrf2-Keap1 pathway in the developing nervous system

In mammals, Nrf2 functions as a master regulator that induces expression of antioxidant and detoxifying genes in response to oxidative stress (Motohashi and Yamamoto, 2004; Sykiotis and Bohmann, 2010). In this study, we identify the Nrf2-Keap1 pathway as an important signaling pathway governing dendrite pruning during neuronal development. We first provided multiple lines of genetic evidence demonstrating that CncC plays a cell-autonomous role in dendrite pruning. Likewise, the CncC transcriptional co-activator MafS is required for dendrite pruning. Moreover, the conserved inhibitor Keap1, which has been reported to degrade CncC/Nrf2 in *Drosophila* and mammals (Itoh et al., 1999; Sykiotis and Bohmann, 2008), negatively regulates dendrite pruning. Mammalian Nrf2 activity can be regulated via multiple inhibitory mechanisms in addition to Keap1. Nrf2 can be recognized by β-TrCP and GSK-3 and targeted for proteasomal degradation (Chowdhry et al., 2013). It would be of interest to test whether *Drosophila* CncC is also negatively regulated by Slimb or Sgg (*Drosophila* homologs of β-TrCP and GSK-3, respectively). Finally, mammalian Nrf2 and worm SKN-1 function as a central node to crosstalk with the insulin pathway (Beyer et al., 2008; Bishop and Guarente, 2007; Tullet et al., 2008). Downregulation of the insulin pathway by ecdysone signaling has been reported to control fly body size (Colombani et al., 2005) and also facilitate dendrite pruning in ddaC neurons (Wong et al., 2013). Future studies are required to identify potential crosstalk between the Nrf2-Keap1 pathway and insulin pathway in dendrite pruning.

A link between the Nrf2-Keap1 pathway and steroid hormone signaling

In this study, we demonstrate that ecdysone signaling is necessary and sufficient to activate the Nrf2-Keap1 pathway by gating the cytoplasmic-to-nuclear translocation of CncC. First, *gstD1-lacZ* was upregulated in ddaC neurons at the prepupal stages, indicating that activation of the Nrf2-Keap1 pathway temporally lags behind activation of ecdysone signaling at the wL3 larval stage. Moreover, *gstD1-lacZ* expression was almost fully abolished when ecdysone signaling was blocked and induced prematurely upon Sox14 overexpression. Interestingly, activation of the Nrf2-Keap1 pathway is mediated by importin-dependent nuclear translocation of CncC. CncC nuclear accumulation was largely abolished in ddaC neurons lacking EcR-B1, Usp, or Sox14 function. Conversely, when ecdysone signaling was hyperactivated, CncC exhibited premature nuclear accumulation at the larval stage. Overall, our results strongly support the conclusion that the Nrf2-Keap1 pathway is activated by ecdysone signaling and promotes dendrite pruning downstream of Sox14 but in parallel to the Mical pathway (see the model in Figure 7K). Importantly, ecdysone signaling has also been reported to regulate lifespan in *Drosophila* (Ahmed et al., 2020; Simon et al., 2003); therefore, this link might have important implications in aging and longevity.

How is the Nrf2-Keap1 pathway activated by ecdysone signaling? One possibility is that ecdysone signaling activates the Nrf2-Keap1 pathway by inducing expression of CncC during larval-to-pupal transition. In support of this possibility, a recent elegant transcriptional profiling study identified *cnc* as one of the most prominent targets of ecdysone signaling in remodeling MB γ neurons, but its function has not been characterized (Alyagor et al., 2018). However, activation of the Nrf2-Keap1 pathway appears to be a more complex process. We found that CncC protein was translocated from the cytoplasm to the nucleus at the prepupal stages, depending on ecdysone signaling. Interestingly, continuous CncC overexpression led to activation of the Nrf2-Keap1 pathway at the early pupal stage but not at larval stages. Failure to activate the Nrf2-Keap1 pathway at the larval stage is likely due to cytoplasmic retention of the overexpressed protein. Hence, cytoplasmic-to-nuclear translocation of CncC is a rate-limiting step for proper activation of the Nrf2-Keap1 pathway. It is conceivable that an unknown cellular switch may also respond to ecdysone signaling to gate shuttling of CncC into nuclei at prepupal stages. The importin complex might function as part of this translocation machinery. Alternatively, ecdysone signaling inhibits the insulin pathway to induce larval crawling and inhibit larval growth during larval-to-pupal transition (Colombani et al., 2005; Yuan et al., 2020). Inhibition of the insulin pathway might trigger cellular stresses that dissociate CncC from Keap1 and, in turn, induce cytoplasmic-to-nuclear translocation of CncC.

A proteasome-dependent role of the Nrf2-Keap1 pathway in dendrite pruning

The Nrf2-Keap1 pathway is the central regulator of the antioxidant response pathway that induces expression of genes encoding antioxidant and detoxifying enzymes in response to oxidative stress (Sykiotis and Bohmann, 2010). Unexpectedly, our systematic investigations indicate that the canonical antioxidant function of CncC is dispensable for dendrite pruning in *Drosophila* (Figure 7K). First, overexpression of various CncC-dependent downstream antioxidant enzymes did not rescue the dendrite pruning defects in *cnc* neurons. Second, unlike the *cncC* mutants, loss of these antioxidant genes did not impair normal dendrite pruning. Third, impaired mitochondrial function, which has been shown to generate high oxidative stress in neurons (Liu et al., 2015), did not inhibit dendrite pruning in ddaC neurons.

Although the antioxidant function has been studied extensively, very few studies so far have shown that CncC and Nrf2 are also important for expression and/or activity of the proteasome (Grimberg et al., 2011; Kwak et al., 2003). Another mammalian ortholog, Nrf1, has been reported to induce compensatory expression of 26S proteasome subunits when proteasome function is impaired in cultured cells (Radhakrishnan et al., 2010; Steffen et al., 2010). However, the physiological roles of this compensatory regulation remain largely unknown. Importantly, we demonstrate here that CncC is required to promote proteasome gene expression and activity in ddaC neurons during development. The proteasome-dependent degradation pathway has been shown to play a key role in neuronal pruning in previous studies (Kuo et al., 2006; Watts et al., 2003; Wong et al., 2013). We found here that poly-ubiquitinated protein

aggregates accumulated in ddaC sensory neurons upon inhibition of the Nrf2-Keap1 pathway. Our real-time PCR assays confirm that CncC is required for transcript levels of the 20S and 19S proteasomal subunits in neurons. Moreover, using the reporter CL1-GFP, we showed a strong increase in proteasomal degradation activity during larval-to-pupal transition. Importantly, by using a newly identified *rpn6-lacZ* reporter line, we substantiate the conclusion that the Nrf2-Keap1 pathway is necessary and sufficient to upregulate expression of proteasomal subunits in ddaC neurons prior to dendrite pruning. However, the size/amount of ubiquitin aggregates in *cncC* mutant neurons appear to be less robust than those upon knockdown of two proteasome subunits, Mov34 and Rpn7. These data suggest that multiple pathways might redundantly regulate transcription of proteasome subunits and that CncC may play a fractional role in their transcription (Figure 7K). It is conceivable that ecdysone signaling might also induce transcription of proteasome subunits via other, still unidentified factors in addition to Nrf2-Keap1 pathway (Figure 7K). The findings from this study and a previous study (Alyagor et al., 2018) also raise interesting questions regarding whether CncC directly activates the transcription of proteasome subunits and whether CncC coordinates with EcR-B1 to simultaneously upregulate almost all proteasomal subunits in remodeling neurons. On the other hand, another study also suggests a feedback loop between CncC and proteasomal degradation because CncC is a substrate of the 26S proteasome in *Drosophila* S2 cells (Grimberg et al., 2011). However, we found that CncC did not accumulate in ubiquitin-positive puncta in the cytoplasm of *mov34* or *rpn7* RNAi ddaC neurons (this study), suggesting that activation of proteasomal degradation during pruning is selective, not toward CncC.

STAR★METHODS

Detailed methods are provided in the online version of this paper and include the following:

- KEY RESOURCES TABLE
- RESOURCE AVAILABILITY
  - Lead contact
  - Materials availability
  - Data and code availability
- EXPERIMENTAL MODEL AND SUBJECT DETAILS
  - Genotypes of the fly strains
- METHOD DETAILS
  - Fly Strains
  - EMS Mutagenesis
  - Generation of various cnc transgenes
  - Generation of mafs mutants via CRISPR/Cas9 technology
  - Generation of anti-CncC antibody
  - Immunohistochemistry and antibodies
  - Live imaging analysis
  - MARCM analysis of da sensory neurons
  - Quantitative real-time PCR (Q-PCR)
  - Quantification of dendrites
  - Quantification of immunostaining
- QUANTIFICATION AND STATISTICAL ANALYSIS

SUPPLEMENTAL INFORMATION

Supplemental information can be found online at https://doi.org/10.1016/j.celrep.2021.109466.

ACKNOWLEDGMENTS

We thank D. Bohmann, H. Deng, B. Eaton, Y. Jan, H. Jasper, T. Kerppola, A.L. Kolodkin, R. Lehmann, W. McGinnis, W. Orr, J.P. Taylor, T. Uemura, the Bloomington Drosophila Stock Center, DSHB (University of Iowa), and VDRC (Austria) for generously providing antibodies and fly stocks. We thank W.L. Yong, Q. Tang, and X. Yao for technical support and other Yu lab members for helpful discussions. This work was funded by Temasek Life Sciences Laboratory Singapore (TLL-2040).

AUTHOR CONTRIBUTIONS

F.Y., L.Y.C., and H.Z. conceived and designed the study. L.Y.C. and H.Z. performed most of the experiments. J.H. conducted some immunostaining experiments. L.Y.C., H.Z., and F.Y. analyzed the data. F.Y. and L.Y.C. wrote the paper.

DECLARATION OF INTERESTS

The authors declare no competing interests.

Received: January 20, 2021
Revised: June 9, 2021
Accepted: July 8, 2021
Published: August 3, 2021

REFERENCES

Ahmed, S.M.H., Maldera, J.A., Krunic, D., Paiva-Silva, G.O., Pénalva, C., Teleman, A.A., and Edgar, B.A. (2020). Fitness trade-offs incurred by ovary-to-gut steroid signalling in Drosophila. Nature *584*, 415–419.

Alyagor, I., Berkun, V., Keren-Shaul, H., Marmor-Kollet, N., David, E., Mayseless, O., Issman-Zecharya, N., Amit, I., and Schuldiner, O. (2018). Combining Developmental and Perturbation-Seq Uncovers Transcriptional Modules Orchestrating Neuronal Remodeling. Dev. Cell *47*, 38–52.e6.

Bence, N.F., Sampat, R.M., and Kopito, R.R. (2001). Impairment of the ubiquitin-proteasome system by protein aggregation. Science *292*, 1552–1555.

Beyer, T.A., Xu, W., Teupser, D., auf dem Keller, U., Bugnon, P., Hildt, E., Thiery, J., Kan, Y.W., and Werner, S. (2008). Impaired liver regeneration in Nrf2 knockout mice: role of ROS-mediated insulin/IGF-1 resistance. EMBO J. *27*, 212–223.

Bishop, N.A., and Guarente, L. (2007). Two neurons mediate diet-restriction-induced longevity in C. elegans. Nature *447*, 545–549.

Boulanger, A., Clouet-Redt, C., Farge, M., Flandre, A., Guignard, T., Fernando, C., Juge, F., and Dura, J.M. (2011). ftz-f1 and Hr39 opposing roles on EcR expression during Drosophila mushroom body neuron remodeling. Nat. Neurosci. *14*, 37–44.

Chowdhry, S., Zhang, Y., McMahon, M., Sutherland, C., Cuadrado, A., and Hayes, J.D. (2013). Nrf2 is controlled by two distinct β-TrCP recognition motifs in its Neh6 domain, one of which can be modulated by GSK-3 activity. Oncogene *32*, 3765–3781.

Colombani, J., Bianchini, L., Layalle, S., Pondeville, E., Dauphin-Villemant, C., Antoniewski, C., Carré, C., Noselli, S., and Léopold, P. (2005). Antagonistic actions of ecdysone and insulins determine final size in Drosophila. Science *310*, 667–670.

Consoulas, C., Duch, C., Bayline, R.J., and Levine, R.B. (2000). Behavioral transformations during metamorphosis: remodeling of neural and motor systems. Brain Res. Bull. *53*, 571–583.

DeGennaro, M., Hurd, T.R., Siekhaus, D.E., Biteau, B., Jasper, H., and Lehmann, R. (2011). Peroxiredoxin stabilization of DE-cadherin promotes primordial germ cell adhesion. Dev. Cell *20*, 233–243.

Deng, H., and Kerppola, T.K. (2014). Visualization of the Drosophila dKeap1-CncC interaction on chromatin illumines cooperative, xenobiotic-specific gene activation. Development *141*, 3277–3288.

Grimberg, K.B., Beskow, A., Lundin, D., Davis, M.M., and Young, P. (2011). Basic leucine zipper protein Cnc-C is a substrate and transcriptional regulator of the Drosophila 26S proteasome. Mol. Cell. Biol. *31*, 897–909.

Grueber, W.B., Ye, B., Moore, A.W., Jan, L.Y., and Jan, Y.N. (2003). Dendrites of distinct classes of Drosophila sensory neurons show different capacities for homotypic repulsion. Curr. Biol. *13*, 618–626.

Hayes, J.D., and Dinkova-Kostova, A.T. (2014). The Nrf2 regulatory network provides an interface between redox and intermediary metabolism. Trends Biochem. Sci. *39*, 199–218.

Hochmuth, C.E., Biteau, B., Bohmann, D., and Jasper, H. (2011). Redox regulation by Keap1 and Nrf2 controls intestinal stem cell proliferation in Drosophila. Cell Stem Cell *8*, 188–199.

Itoh, K., Wakabayashi, N., Katoh, Y., Ishii, T., Igarashi, K., Engel, J.D., and Yamamoto, M. (1999). Keap1 represses nuclear activation of antioxidant responsive elements by Nrf2 through binding to the amino-terminal Neh2 domain. Genes Dev. *13*, 76–86.

Kanamori, T., Kanai, M.I., Dairyo, Y., Yasunaga, K., Morikawa, R.K., and Emoto, K. (2013). Compartmentalized calcium transients trigger dendrite pruning in Drosophila sensory neurons. Science *340*, 1475–1478.

Kanamori, T., Togashi, K., Koizumi, H., and Emoto, K. (2015). Dendritic Remodeling: Lessons from Invertebrate Model Systems. Int. Rev. Cell Mol. Biol. *318*, 1–25.

Kirilly, D., Gu, Y., Huang, Y., Wu, Z., Bashirullah, A., Low, B.C., Kolodkin, A.L., Wang, H., and Yu, F. (2009). A genetic pathway composed of Sox14 and Mical governs severing of dendrites during pruning. Nat. Neurosci. *12*, 1497–1505.

Kirilly, D., Wong, J.J., Lim, E.K., Wang, Y., Zhang, H., Wang, C., Liao, Q., Wang, H., Liou, Y.C., Wang, H., and Yu, F. (2011). Intrinsic epigenetic factors cooperate with the steroid hormone ecdysone to govern dendrite pruning in Drosophila. Neuron *72*, 86–100.

Kobayashi, M., Itoh, K., Suzuki, T., Osanai, H., Nishikawa, K., Katoh, Y., Takagi, Y., and Yamamoto, M. (2002). Identification of the interactive interface and phylogenic conservation of the Nrf2-Keap1 system. Genes Cells *7*, 807–820.

Kreko-Pierce, T., and Eaton, B.A. (2017). The *Drosophila* LC8 homolog *cut up* specifies the axonal transport of proteasomes. J. Cell Sci. *130*, 3388–3398.

Kuo, C.T., Jan, L.Y., and Jan, Y.N. (2005). Dendrite-specific remodeling of Drosophila sensory neurons requires matrix metalloproteases, ubiquitin-proteasome, and ecdysone signaling. Proc. Natl. Acad. Sci. USA *102*, 15230–15235.

Kuo, C.T., Zhu, S., Younger, S., Jan, L.Y., and Jan, Y.N. (2006). Identification of E2/E3 ubiquitinating enzymes and caspase activity regulating Drosophila sensory neuron dendrite pruning. Neuron *51*, 283–290.

Kwak, M.K., Wakabayashi, N., Greenlaw, J.L., Yamamoto, M., and Kensler, T.W. (2003). Antioxidants enhance mammalian proteasome expression through the Keap1-Nrf2 signaling pathway. Mol. Cell. Biol. *23*, 8786–8794.

Lee, T., Lee, A., and Luo, L. (1999). Development of the Drosophila mushroom bodies: sequential generation of three distinct types of neurons from a neuroblast. Development *126*, 4065–4076.

Lee, T., Marticke, S., Sung, C., Robinow, S., and Luo, L. (2000). Cell-autonomous requirement of the USP/EcR-B ecdysone receptor for mushroom body neuronal remodeling in Drosophila. Neuron *28*, 807–818.

Liu, L., Zhang, K., Sandoval, H., Yamamoto, S., Jaiswal, M., Sanz, E., Li, Z., Hui, J., Graham, B.H., Quintana, A., and Bellen, H.J. (2015). Glial lipid droplets and ROS induced by mitochondrial defects promote neurodegeneration. Cell *160*, 177–190.

Loncle, N., and Williams, D.W. (2012). An interaction screen identifies headcase as a regulator of large-scale pruning. J. Neurosci. *32*, 17086–17096.

Luo, L., and O'Leary, D.D. (2005). Axon retraction and degeneration in development and disease. Annu. Rev. Neurosci. *28*, 127–156.

Marchetti, G., and Tavosanis, G. (2017). Steroid Hormone Ecdysone Signaling Specifies Mushroom Body Neuron Sequential Fate via Chinmo. Curr. Biol. *27*, 3017–3024.e4.

Matsubara, D., Horiuchi, S.Y., Shimono, K., Usui, T., and Uemura, T. (2011). The seven-pass transmembrane cadherin Flamingo controls dendritic self-avoidance via its binding to a LIM domain protein, Espinas, in Drosophila sensory neurons. Genes Dev. *25*, 1982–1996.

McGinnis, N., Ragnhildstveit, E., Veraksa, A., and McGinnis, W. (1998). A cap 'n' collar protein isoform contains a selective Hox repressor function. Development *125*, 4553–4564.

Milton, V.J., Jarrett, H.E., Gowers, K., Chalak, S., Briggs, L., Robinson, I.M., and Sweeney, S.T. (2011). Oxidative stress induces overgrowth of the Drosophila neuromuscular junction. Proc. Natl. Acad. Sci. USA *108*, 17521–17526.

Mohler, J., Mahaffey, J.W., Deutsch, E., and Vani, K. (1995). Control of Drosophila head segment identity by the bZIP homeotic gene cnc. Development *121*, 237–247.

Motohashi, H., and Yamamoto, M. (2004). Nrf2-Keap1 defines a physiologically important stress response mechanism. Trends Mol. Med. *10*, 549–557.

O'Leary, D.D., and Koester, S.E. (1993). Development of projection neuron types, axon pathways, and patterned connections of the mammalian cortex. Neuron *10*, 991–1006.

Orr, W.C., Radyuk, S.N., Prabhudesai, L., Toroser, D., Benes, J.J., Luchak, J.M., Mockett, R.J., Rebrin, I., Hubbard, J.G., and Sohal, R.S. (2005). Overexpression of glutamate-cysteine ligase extends life span in Drosophila melanogaster. J. Biol. Chem. *280*, 37331–37338.

Otis, K.O., Thompson, K.R., and Martin, K.C. (2006). Importin-mediated nuclear transport in neurons. Curr. Opin. Neurobiol. *16*, 329–335.

Owusu-Ansah, E., and Banerjee, U. (2009). Reactive oxygen species prime Drosophila haematopoietic progenitors for differentiation. Nature *461*, 537–541.

Pandey, U.B., Nie, Z., Batlevi, Y., McCray, B.A., Ritson, G.P., Nedelsky, N.B., Schwartz, S.L., DiProspero, N.A., Knight, M.A., Schuldiner, O., et al. (2007). HDAC6 rescues neurodegeneration and provides an essential link between autophagy and the UPS. Nature *447*, 859–863.

Port, F., Chen, H.M., Lee, T., Bullock, S.L., et al. (2014). Optimized CRISPR/Cas tools for efficient germline and somatic genome engineering in Drosophila. Proc. Natl. Acad Sci. U S A *111* (*29*), E2967–E2976. https://doi.org/10.1073/pnas.1405500111.

Radhakrishnan, S.K., Lee, C.S., Young, P., Beskow, A., Chan, J.Y., and Deshaies, R.J. (2010). Transcription factor Nrf1 mediates the proteasome recovery pathway after proteasome inhibition in mammalian cells. Mol. Cell *38*, 17–28.

Radyuk, S.N., Sohal, R.S., and Orr, W.C. (2003). Thioredoxin peroxidases can foster cytoprotection or cell death in response to different stressors: over- and under-expression of thioredoxin peroxidase in Drosophila cells. Biochem. J. *371*, 743–752.

Riccomagno, M.M., and Kolodkin, A.L. (2015). Sculpting neural circuits by axon and dendrite pruning. Annu. Rev. Cell Dev. Biol. *31*, 779–805.

Riccomagno, M.M., Hurtado, A., Wang, H., Macopson, J.G., Griner, E.M., Betz, A., Brose, N., Kazanietz, M.G., and Kolodkin, A.L. (2012). The RacGAP β2-Chimaerin selectively mediates axonal pruning in the hippocampus. Cell *149*, 1594–1606.

Rodriguez-Fernandez, I.A., Qi, Y., and Jasper, H. (2019). Loss of a proteostatic checkpoint in intestinal stem cells contributes to age-related epithelial dysfunction. Nat. Commun. *10*, 1050.

Schuldiner, O., and Yaron, A. (2015). Mechanisms of developmental neurite pruning. Cell. Mol. Life Sci. *72*, 101–119.

Schuldiner, O., Berdnik, D., Levy, J.M., Wu, J.S., Luginbuhl, D., Gontang, A.C., and Luo, L. (2008). piggyBac-based mosaic screen identifies a postmitotic

function for cohesin in regulating developmental axon pruning. Dev. Cell *14*, 227–238.

Simon, A.F., Shih, C., Mack, A., and Benzer, S. (2003). Steroid control of longevity in Drosophila melanogaster. Science *299*, 1407–1410.

Steffen, J., Seeger, M., Koch, A., and Krüger, E. (2010). Proteasomal degradation is transcriptionally controlled by TCF11 via an ERAD-dependent feedback loop. Mol. Cell *40*, 147–158.

Sykiotis, G.P., and Bohmann, D. (2008). Keap1/Nrf2 signaling regulates oxidative stress tolerance and lifespan in Drosophila. Dev. Cell *14*, 76–85.

Sykiotis, G.P., and Bohmann, D. (2010). Stress-activated cap'n'collar transcription factors in aging and human disease. Sci. Signal. *3*, re3.

Tang, G., Gudsnuk, K., Kuo, S.H., Cotrina, M.L., Rosoklija, G., Sosunov, A., Sonders, M.S., Kanter, E., Castagna, C., Yamamoto, A., et al. (2014). Loss of mTOR-dependent macroautophagy causes autistic-like synaptic pruning deficits. Neuron *83*, 1131–1143.

Tang, Q., Rui, M., Bu, S., Wang, Y., Chew, L.Y., and Yu, F. (2020). A microtubule polymerase is required for microtubule orientation and dendrite pruning in Drosophila. EMBO J. *39*, e103549.

Tapia, J.C., Wylie, J.D., Kasthuri, N., Hayworth, K.J., Schalek, R., Berger, D.R., Guatimosim, C., Seung, H.S., and Lichtman, J.W. (2012). Pervasive synaptic branch removal in the mammalian neuromuscular system at birth. Neuron *74*, 816–829.

Terman, J.R., Mao, T., Pasterkamp, R.J., Yu, H.H., and Kolodkin, A.L. (2002). MICALs, a family of conserved flavoprotein oxidoreductases, function in plexin-mediated axonal repulsion. Cell *109*, 887–900.

Thummel, C.S. (1996). Flies on steroids–Drosophila metamorphosis and the mechanisms of steroid hormone action. Trends Genet. *12*, 306–310.

Towers, C.G., Fitzwalter, B.E., Regan, D., Goodspeed, A., Morgan, M.J., Liu, C.W., Gustafson, D.L., and Thorburn, A. (2019). Cancer Cells Upregulate NRF2 Signaling to Adapt to Autophagy Inhibition. Dev. Cell *50*, 690–703.e6.

Truman, J.W. (1990). Metamorphosis of the central nervous system of Drosophila. J. Neurobiol. *21*, 1072–1084.

Tullet, J.M., Hertweck, M., An, J.H., Baker, J., Hwang, J.Y., Liu, S., Oliveira, R.P., Baumeister, R., and Blackwell, T.K. (2008). Direct inhibition of the longevity-promoting factor SKN-1 by insulin-like signaling in C. elegans. Cell *132*, 1025–1038.

Veraksa, A., McGinnis, N., Li, X., Mohler, J., and McGinnis, W. (2000). Cap 'n' collar B cooperates with a small Maf subunit to specify pharyngeal development and suppress deformed homeotic function in the Drosophila head. Development *127*, 4023–4037.

Wang, B., Liu, Q., Shan, H., Xia, C., and Liu, Z. (2015). Nrf2 inducer and cncC overexpression attenuates neurodegeneration due to α-synuclein in Drosophila. Biochem. Cell Biol. *93*, 351–358.

Wang, Q., Wang, Y., and Yu, F. (2018). Yif1 associates with Yip1 on Golgi and regulates dendrite pruning in sensory neurons during Drosophila metamorphosis. Development *145*, dev164475.

Watts, R.J., Hoopfer, E.D., and Luo, L. (2003). Axon pruning during Drosophila metamorphosis: evidence for local degeneration and requirement of the ubiquitin-proteasome system. Neuron *38*, 871–885.

Williams, D.W., and Truman, J.W. (2005). Cellular mechanisms of dendrite pruning in Drosophila: insights from in vivo time-lapse of remodeling dendritic arborizing sensory neurons. Development *132*, 3631–3642.

Wong, J.J., Li, S., Lim, E.K., Wang, Y., Wang, C., Zhang, H., Kirilly, D., Wu, C., Liou, Y.C., Wang, H., and Yu, F. (2013). A Cullin1-based SCF E3 ubiquitin ligase targets the InR/PI3K/TOR pathway to regulate neuronal pruning. PLoS Biol. *11*, e1001657.

Yaron, A., and Schuldiner, O. (2016). Common and Divergent Mechanisms in Developmental Neuronal Remodeling and Dying Back Neurodegeneration. Curr. Biol. *26*, R628–R639.

Yu, F., and Schuldiner, O. (2014). Axon and dendrite pruning in Drosophila. Curr. Opin. Neurobiol. *27*, 192–198.

Yu, X.M., Gutman, I., Mosca, T.J., Iram, T., Ozkan, E., Garcia, K.C., Luo, L., and Schuldiner, O. (2013). Plum, an immunoglobulin superfamily protein, regulates axon pruning by facilitating TGF-β signaling. Neuron *78*, 456–468.

Yuan, D., Zhou, S., Liu, S., Li, K., Zhao, H., Long, S., Liu, H., Xie, Y., Su, Y., Yu, F., and Li, S. (2020). The AMPK-PP2A axis in insect fat body is activated by 20-hydroxyecdysone to antagonize insulin/IGF signaling and restrict growth rate. Proc. Natl. Acad. Sci. USA *117*, 9292–9301.

Zhang, D.D., and Hannink, M. (2003). Distinct cysteine residues in Keap1 are required for Keap1-dependent ubiquitination of Nrf2 and for stabilization of Nrf2 by chemopreventive agents and oxidative stress. Mol. Cell. Biol. *23*, 8137–8151.

Zhang, H., Wang, Y., Wong, J.J., Lim, K.L., Liou, Y.C., Wang, H., and Yu, F. (2014). Endocytic pathways downregulate the L1-type cell adhesion molecule neuroglian to promote dendrite pruning in Drosophila. Dev. Cell *30*, 463–478.

Zheng, X., Wang, J., Haerry, T.E., Wu, A.Y., Martin, J., O'Connor, M.B., Lee, C.H., and Lee, T. (2003). TGF-beta signaling activates steroid hormone receptor expression during neuronal remodeling in the Drosophila brain. Cell *112*, 303–315.

STAR★METHODS

KEY RESOURCES TABLE

REAGENT or RESOURCE	SOURCE	IDENTIFIER
Antibodies		
Mouse polyclonal anti-CncC (P2)	This paper	N/A
Mouse polyclonal anti-CncC (P4)	This paper	N/A
Mouse monoclonal anti-β-Galactosidase	Promega	Cat#378A; RRID: AB_2313752
Mouse monoclonal mono- and poly-ubiquitinated conjugates antibody (FK2)	Enzo Life Sciences	Cat# BML-PW8810, RRID: AB_10541840
Rat monoclonal anti-HA	Roche	Cat# 11867423001, RRID:_AB_390918
Mouse monoclonal anti-EcR-B1	Developmental Studies Hybridoma Bank	Cat# AD4.4; RRID: AB_2154902
Guinea Pig polyclonal anti-Mical	Yu Lab, Temasek Life Sciences Laboratory, Singapore (Kirilly et al., 2009)	N/A
Cy3 AffiniPure goat polyclonal anti-mouse IgG (H+L)	Jackson ImmunoResearch Laboratories	Cat#115-165-003; RRID: AB_2338680
Cy3 AffiniPure goat polyclonal anti-rat IgG (H+L)	Jackson ImmunoResearch Laboratories	Cat#112-165-003; RRID: AB_2338240
Cy3 AffiniPure goat polyclonal anti-guinea pig IgG (H+L)	Jackson ImmunoResearch Laboratories	Cat#106-165-003; RRID: AB_2337423
Alexa Fluor® 647 AffiniPure Goat Anti-Horseradish Peroxidase	Jackson ImmunoResearch Laboratories	Cat#123-605-021; RRID: AB_2338967
Chemicals, peptides, and recombinant proteins		
TRIZOL RNA isolation Reagent	Invitrogen	Cat#15596026
Maxima SYBR Green/ROX qPCR Master Mix (2X)	Fermentas	Cat#K0221
Formaldehyde	Polysciences Inc.	Cat#NC9200219
Glycerol	Invitrogen	Cat#15514011
Vectashield	Vector Laboratories	Cat#H-1000
Critical commercial assays		
Axygen Plasmid Miniprep Kit	Axygen	Cat#AP-MN-P-250
pENTR™/D-TOPO™ Cloning Kit	Invitrogen	Cat#K240020
QuikChange Lightning Site-directed Mutagenesis Kit	Agilent Technologies	Cat#210518
Gateway™ LR Clonase™ II Enzyme mix	Invitrogen	Cat#11791020
Experimental models: Organisms/strains		
Drosophila melanogaster: UAS-Mical$^{N\text{-}ter}$	Terman et al., 2002	N/A
Drosophila melanogaster: ppk-Gal4 (Chr. II and III)	Grueber et al., 2003	N/A
Drosophila melanogaster: SOP-flp (Chr. II and III)	Matsubara et al., 2011	N/A
Drosophila melanogaster: cnc^{K6}	Veraksa et al., 2000	N/A
Drosophila melanogaster: cnc^{VL110}	Veraksa et al., 2000	N/A
Drosophila melanogaster: UAS-CncB	Veraksa et al., 2000	N/A
Drosophila melanogaster: UAS-Keap1	Sykiotis and Bohmann, 2008	N/A
Drosophila melanogaster: UAS-Keap1-HA	Sykiotis and Bohmann, 2008	N/A
Drosophila melanogaster: keap1^{036}	Sykiotis and Bohmann, 2008	N/A
Drosophila melanogaster: gstD1-lacZ	Sykiotis and Bohmann, 2008	N/A
Drosophila melanogaster: UAS-CncC	Sykiotis and Bohmann, 2008	N/A

(*Continued on next page*)

Continued

REAGENT or RESOURCE	SOURCE	IDENTIFIER
Drosophila melanogaster: UAS-Jafrac1	DeGennaro et al., 2011; Hochmuth et al., 2011	N/A
Drosophila melanogaster: UAS-Gclm	Orr et al., 2005	N/A
Drosophila melanogaster: UAS-Gclc	Orr et al., 2005	N/A
Drosophila melanogaster: UAS-Sox14	Kirilly et al., 2009	N/A
Drosophila melanogaster: UAS-CL1-GFP	Pandey et al., 2007	N/A
Drosophila melanogaster: UAS-Prosβ5-RFP	Kreko-Pierce and Eaton, 2017	N/A
Drosophila melanogaster: cnc^{1223}	This study	N/A
Drosophila melanogaster: mafs$^{9-1}$	This study	N/A
Drosophila melanogaster: mafs$^{8-3}$	This study	N/A
Drosophila melanogaster: UAS-mCD8::GFP (Chr. II and III)	Bloomington Stock Centre (BDSC)	RRID:BDSC_5130; RRID:BDSC_5137
Drosophila melanogaster: FRTG13	BDSC	RRID:BDSC_1956
Drosophila melanogaster: FRT82B	BDSC	RRID:BDSC_2035
Drosophila melanogaster: UAS-Dicer2 (Chr. II and III)	BDSC	RRID:BDSC_24650; RRID:BDSC_24651
Drosophila melanogaster: FRT82B, *tubP-Gal80*	BDSC	RRID:BDSC_5135
Drosophila melanogaster: FRTG13, *tubP-Gal80*	BDSC	RRID:BDSC_5140
Drosophila melanogaster: elav-Gal4^{C155}	BDSC	RRID:BDSC_458
Drosophila melanogaster: cnc RNAi #2	BDSC	RRID:BDSC_40854
Drosophila melanogaster: rpn7 RNAi	BDSC	RRID:BDSC_34787
Drosophila melanogaster: keap1 RNAi #2	BDSC	RRID:BDSC_40932
Drosophila melanogaster: UAS-EcR^{DN}	BDSC	RRID:BDSC_6872
Drosophila melanogaster: imp-β RNAi #1	BDSC	RRID:BDSC_27567
Drosophila melanogaster: imp-β RNAi #2	BDSC	RRID:BDSC_31242
Drosophila melanogaster: Jafrac1^{KG05372}	BDSC	RRID:BDSC_14440
Drosophila melanogaster: sod1^{n1}	BDSC	RRID:BDSC_24492
Drosophila melanogaster: sod2$^{\Delta 02}$	BDSC	RRID:BDSC_27643
Drosophila melanogaster: sod2^{n283}	BDSC	RRID:BDSC_34060
Drosophila melanogaster: UAS-Sod1	BDSC	RRID:BDSC_33605
Drosophila melanogaster: UAS-Sod2	BDSC	RRID:BDSC_24494
Drosophila melanogaster: UAS-hSod1	BDSC	RRID:BDSC_33606
Drosophila melanogaster: marf^{B}	BDSC	RRID:BDSC_67154
Drosophila melanogaster: aats-met^{FB}	BDSC	RRID:BDSC_39747
Drosophila melanogaster: UAS-Catalase	BDSC	RRID:BDSC_24621
Drosophila melanogaster: rpn6-LacZ (*rpn6^{k00103}*)	BDSC	RRID:BDSC_10465
Drosophila melanogaster: cnc RNAi #1	Vienna *Drosophila* RNAi Centre (VDRC)	GD-37674
Drosophila melanogaster: cnc RNAi #3	VDRC	KK-101235
Drosophila melanogaster: keap1 RNAi #1	VDRC	SH-330323
Drosophila melanogaster: usp RNAi	VDRC	GD-16893
Drosophila melanogaster: sox14 RNAi	VDRC	GD-10856
Drosophila melanogaster: mical RNAi	VDRC	GD-46097
Drosophila melanogaster: mov34 RNAi	VDRC	GD-26183
Drosophila melanogaster: UAS-CncA-HA	FlyORF	F000602
Drosophila melanogaster: UAS-Mafs-HA	FlyORF	F000012
Drosophila melanogaster: cat^{n1}	Kyoto Stock Centre (DGRC)	DGRC_107554

(*Continued on next page*)

Continued

REAGENT or RESOURCE	SOURCE	IDENTIFIER
Drosophila melanogaster: cat^{n4}	DGRC	DGRC_101586
Drosophila melanogaster: ND-42 RNAi #1	National Institute of Genetics (NIG)	NIG_6343R-1
Drosophila melanogaster: ND-42 RNAi #2	NIG	NIG_6343R-2
Drosophila melanogaster: ND-75 RNAi	NIG	NIG_2286-2
Oligonucleotides		
See Table S1		N/A
pCFD4	Addgene	Cat#49411
pTW	DGRC	Cat#1129
pTVW	DGRC	Cat#1091
pQE30	QIAGEN	Cat#32915
pGEX 4T-1	Amersham Pharmacia Biotech	Cat#27-4580-01
GCACCACTTTCGCCATGTCCAA TTCCGGATATTACCGATGACGATT TGGTGAGCATTTCGGTAAGGGAT CTTAATCGGACCCTCAAGATGCGT GGCCTGAACCGCGAGGAGATCG TTCGGATGAA	This paper	For generating *mafs* CRISPR mutant
CGTGGTGAAAGCGGTACAGG TTAAGGCCTATAATGGCTACTG CTAAACCACTCGTAAAGCCATTC CCTAGAATTAGCCTGGGAGTTC TACGCACCGGACTTGGCGCTCC TCTAGCAAGCCTACTT	This paper	For generating *mafs* CRISPR mutant
Recombinant DNA		
Plasmid: pTW-CncC $^{\Delta A}$	This paper	N/A
Plasmid: pTW-CncC $^{\Delta B}$	This paper	N/A
Plasmid: pTW-CncC $^{\Delta DLG+ETGE}$	This paper	N/A
Plasmid: pTVW-CncC $^{\Delta NLS}$	This paper	N/A
Plasmid: pQE30-CncC(P2)	This paper	N/A
Plasmid: pGEX-CncC(P4)	This paper	N/A
Software and algorithms		
Adobe Photoshop	Adobe	https://www.adobe.com/products/photoshop.html
Adobe Illustrator	Adobe	https://www.adobe.com/products/illustrator.html
Fiji (ImageJ)	NIH	https://imagej.net/software/fiji/downloads
GraphPad Prism 8	GraphPad	https://www.graphpad.com/scientific-software/prism/
Excel	Microsoft	https://www.microsoft.com/en-us/microsoft-365/excel
Olympus FV3000 confocal microscopy	Olympus	https://www.olympus-lifescience.com/en/laser-scanning/fv3000/
Leica TCS SP2 confocal microscopy	Leica	https://www.leica-microsystems.com/products/confocal-microscopes/p/leica-tcs-sp2/

RESOURCE AVAILABILITY

Lead contact

Further information and requests for resource and reagents should be directed to and will be fulfilled by the lead contact, Fengwei Yu (fengwei@tll.org.sg)

Materials availability

Most materials are commercially available. All unique reagents generated in this study are available from the lead contact without restriction.

Data and code availability

This study did not generate any codes or large datasets.

EXPERIMENTAL MODEL AND SUBJECT DETAILS

All *Drosophila* stocks and crosses were maintained in standard cornmeal media at 25°C. All fly genotypes used in this study are listed in the key resources table.

Genotypes of the fly strains

Figure 1**: (B)** w*; ppk-Gal4, UAS-mCD8GFP, SOP-flp / +; FRT82B / FRT82B, tubP-Gal80. **(C)** w*; ppk-Gal4, UAS-mCD8GFP, SOP-flp / +; FRT82B, cnc^{1223}/ FRT82B, tubP-Gal80. **(D)** w*; ppk-Gal4, UAS-mCD8GFP, SOP-flp / +; FRT82B, cnc^{K6} / FRT82B, tubP-Gal80. **(E)** w*; ppk-Gal4, UAS-mCD8GFP, SOP-flp / +; FRT82B, cnc^{VL110} / FRT82B, tubP-Gal80. **(F)** w*; ppk-Gal4, UAS-mCD8GFP, UAS-Dcr2 / ppk-Gal4, UAS-mCD8GFP, UAS-Dcr2; UAS-cnc RNAi #1 / UAS-cnc RNAi #1. **(G)** w*; UAS-cnc RNAi #2 / UAS-cnc RNAi #2; ppk-Gal4, UAS-CD8GFP / ppk-Gal4, UAS-CD8GFP. **(H)** w*; UAS-cnc RNAi #3 / UAS-cnc RNAi #3; ppk-Gal4, UAS-CD8GFP, UAS-Dcr2 / ppk-Gal4, UAS-CD8GFP, UAS-Dcr2.

Figure 2**: (B)** w*; ppk-Gal4, UAS-mCD8GFP, SOP-flp / +; FRT82B, cnc^{1223}/ FRT82B, tubP-Gal80. **(C)** w*; ppk-Gal4, UAS-mCD8GFP, SOP-flp / +; FRT82B, cnc^{1223}, UAS-CncA / FRT82B, tubP-Gal80. **(D)** w*; ppk-Gal4, UAS-mCD8GFP, SOP-flp / UAS-CncB; FRT82B, cnc^{1223} / FRT82B, tubP-Gal80. **(E)** w*; ppk-Gal4, UAS-mCD8GFP, SOP-flp / +; FRT82B, cnc^{1223}, UAS-CncC / FRT82B, tubP-Gal80. **(F)** w*; ppk-Gal4, UAS-mCD8GFP, SOP-flp / UAS-$CncC^{\Delta A}$; FRT82B, cnc^{1223} / FRT82B, tubP-Gal80. **(G)** w*; ppk-Gal4, UAS-mCD8GFP, SOP-flp / UAS-$CncC^{\Delta B}$; FRT82B, cnc^{1223} / FRT82B, tubP-Gal80. **(H)** w*; ppk-Gal4, UAS-mCD8GFP, SOP-flp / UAS-$CncC^{\Delta NLS}$; FRT82B, cnc^{1223} / FRT82B, tubP-Gal80. **(I)** w*; ppk-Gal4, UAS-mCD8GFP, SOP-flp / UAS-$CncC^{-\Delta}$DLG+ETGE; FRT82B, cnc^{1223} / FRT82B, tubP-Gal80.

Figure 3**: (B)** w*; FRTG13 / FRTG13, tubP-Gal80; ppk-Gal4, UAS-mCD8GFP, SOP-flp / +. **(C)** w*; FRTG13, $mafs^{9-1}$ / FRTG13, tubP-Gal80; ppk-Gal4, UAS-mCD8GFP, SOP-flp / +. **(D)** w*; FRTG13, $mafs^{8-3}$ / FRTG13, tubP-Gal80; ppk-Gal4, UAS-mCD8GFP, SOP-flp / +. **(E)** w*; FRTG13, $mafs^{9-1}$ / FRTG13, tubP-Gal80; ppk-Gal4, UAS-mCD8GFP, SOP-flp / UAS-Mafs-HA. **(F)** w*; FRTG13, $mafs^{8-3}$ / FRTG13, tubP-Gal80; ppk-Gal4, UAS-mCD8GFP, SOP-flp / UAS-Mafs-HA. **(G)** w*; ppk-Gal4 / ppk-Gal4; ppk-Gal4, UAS-mCD8GFP / ppk-Gal4, UAS-mCD8GFP. **(H)** w*; ppk-Gal4, UAS-Keap1-HA / ppk-Gal4, UAS-Keap1-HA; ppk-Gal4, UAS-mCD8GFP / ppk-Gal4, UAS-mCD8GFP. **(I)** w*; ppk-Gal4, UAS-mCD8GFP, SOP-flp / +; FRT82B, cnc^{1223}/ FRT82B, tubP-Gal80. **(J)** w*; ppk-Gal4, UAS-Keap1-HA / ppk-Gal4, UAS-mCD8GFP, SOP-flp; FRT82B / FRT82B, tubP-Gal80. **(K)** w*; ppk-Gal4, UAS-Keap1-HA / ppk-Gal4, UAS-mCD8GFP, SOP-flp; FRT82B, cnc^{1223} / FRT82B, tubP-Gal80.

Figure 4**: (A)** w*; gstD-lacZ / gstD-lacZ; ppk-Gal4, UAS-CD8GFP / ppk-Gal4, UAS-CD8GFP. **(B) Ctrl RNAi:** w*; gstD-lacZ / ppk-Gal4, UAS-CD8GFP, UAS-Dcr2; ppk-Gal4, UAS-CD8GFP / UAS-Control RNAi. **cnc RNAi #1:** w*; gstD-lacZ / ppk-Gal4, UAS-CD8GFP, UAS-Dcr2; ppk-Gal4, UAS-CD8GFP / UAS-cnc RNAi #1. **cnc RNAi #2:** w*; gstD-lacZ / UAS-cnc RNAi #2; ppk-Gal4, UAS-CD8GFP / ppk-Gal4, UAS-CD8GFP. **(C) O/E Control:** w*; gstD-lacZ / ppk-Gal4, UAS-CD8GFP; ppk-Gal4, UAS-CD8GFP / UAS-$Mical^{NT}$. **O/E Keap1-HA:** w*; gstD-lacZ / ppk-Gal4, UAS-Keap1-HA; ppk-Gal4, UAS-CD8GFP / ppk-Gal4, UAS-CD8GFP. **O/E CncC:** w*; gstD-lacZ / ppk-Gal4, UAS-CD8GFP; ppk-Gal4, UAS-CD8GFP / UAS-CncC. **(D) Ctrl RNAi:** w*; gstD-lacZ / +; ppk-Gal4, UAS-CD8GFP / UAS-Control RNAi. **keap1 RNAi #1:** w*; gstD-lacZ / UAS-keap1 RNAi #1; ppk-Gal4, UAS-CD8GFP / +. **keap1 RNAi #2:** w*; gstD-lacZ / UAS-keap1 RNAi #2; ppk-Gal4, UAS-CD8GFP / +. **(E) O/E Control:** w*; gstD-lacZ / ppk-Gal4, UAS-CD8GFP; ppk-Gal4, UAS-CD8GFP / UAS-$Mical^{NT}$. **O/E EcR^{DN}:** w*; gstD-lacZ / UAS-EcR^{DN}; ppk-Gal4, UAS-CD8GFP / ppk-Gal4, UAS-CD8GFP. **O/E Sox14:** w*; gstD-lacZ / ppk-Gal4, UAS-CD8GFP; ppk-Gal4, UAS-CD8GFP / UAS-Sox14. **(F) Ctrl RNAi:** w*; gstD-lacZ / +; ppk-Gal4, UAS-CD8GFP, UAS-Dcr2/ UAS-Control RNAi. **usp RNAi:** w*; gstD-lacZ / +; ppk-Gal4, UAS-CD8GFP, UAS-Dcr2 / UAS-usp RNAi. **sox14 RNAi:** w*; gstD-lacZ / ppk-Gal4, UAS-CD8GFP, UAS-Dcr2; ppk-Gal4, UAS-CD8GFP / UAS-sox14 RNAi.

Figure 5**: (A)** w*; ; ppk-Gal4, UAS-CD8GFP / ppk-Gal4, UAS-CD8GFP. **(B) Ctrl RNAi:** w*; ppk-Gal4 / + ; ppk-Gal4, UAS-CD8GFP / UAS-Control RNAi. **keap1 RNAi #1:** w*; ppk-Gal4 / UAS-keap1 RNAi #1; ppk-Gal4, UAS-CD8GFP / +. **O/E Control**: w*; ppk-Gal4, UAS-CD8GFP / ppk-Gal4, UAS-CD8GFP; UAS-$Mical^{NT}$ / UAS-$Mical^{NT}$. **O/E Keap1:** w*; ppk-Gal4, UAS-CD8GFP / ppk-Gal4, UAS-CD8GFP; UAS-Keap1 / UAS-Keap1. **(C) Ctrl RNAi:** w*; ppk-Gal4, UAS-CD8GFP / +; UAS-Dcr2 / UAS-Control RNAi. **imp-β RNAi (#1):** w*; ppk-Gal4, UAS-CD8GFP / +; UAS-Dcr2 / UAS-imp-β RNAi #1. **EcR RNAi:** w*; ppk-Gal4, UAS-CD8GFP / +; UAS-Dcr2 / UAS-EcR RNAi. **sox14 RNAi:** w*; ppk-Gal4, UAS-CD8GFP / +; UAS-Dcr2 / UAS-sox14 RNAi. **(D) O/E Control**: w*; ppk-Gal4, UAS-CD8GFP / ppk-Gal4, UAS-CD8GFP; UAS-$Mical^{NT}$ / UAS-$Mical^{NT}$. **O/E Sox14**: w*; ppk-Gal4, UAS-CD8GFP / ppk-Gal4, UAS-CD8GFP; UAS-Sox14 / UAS-Sox14.

Figure 6**: (A)** w*; ppk-Gal4, UAS-CD8GFP, UAS-Dcr2 / +; UAS-cnc RNAi #1 / UAS-$Mical^{NT}$. **(B)** w*; ppk-Gal4, UAS-CD8GFP, UAS-Dcr2 / UAS-Sod1; UAS-cnc RNAi #1 / +. **(C)** w*; ppk-Gal4, UAS-CD8GFP, UAS-Dcr2 / UAS-Sod2; UAS-cnc RNAi #1 / +. **(D)** w*; ppk-Gal4, UAS-CD8GFP, UAS-Dcr2 / +; UAS-cnc RNAi #1 / UAS-hSod1. **(E)** w*; ppk-Gal4, UAS-CD8GFP, UAS-Dcr2 / UAS-catalase;

UAS-cnc RNAi #1 / +. **(F)** w*; ppk-Gal4, UAS-CD8GFP, UAS-Dcr2 / UAS-Jafrac1; UAS-cnc RNAi #1 / +. **(G)** w*; ppk-Gal4, UAS-mCD8GFP, SOP-flp / +; FRT82B, cnc^{1223}/ FRT82B, tubP-Gal80. **(H)** w*; ppk-Gal4, UAS-mCD8GFP, SOP-flp / UAS-Sod1; FRT82B, cnc^{1223}/ FRT82B, tubP-Gal80. **(I)** w*; ppk-Gal4, UAS-mCD8GFP, SOP-flp / UAS-Gclc; FRT82B, cnc^{1223}/ FRT82B, tubP-Gal80. **(J)** w*; ppk-Gal4, UAS-mCD8GFP, SOP-flp / UAS-Gclm; FRT82B, cnc^{1223}/ FRT82B, tubP-Gal80.

Figure 7**: (A) Ctrl RNAi:** w*; ppk-Gal4, UAS-CD8GFP, UAS-Dcr2 / ppk-Gal4, UAS-CD8GFP, UAS-Dcr2; UAS-Control RNAi / UAS-Control RNAi. **cnc RNAi #1**: w*; ppk-Gal4, UAS-CD8GFP, UAS-Dcr2 / ppk-Gal4, UAS-CD8GFP, UAS-Dcr2; UAS-cnc RNAi #1 / UAS-cnc RNAi #1. **cnc RNAi #2**: w*; UAS-cnc RNAi #2 / UAS-cnc RNAi #2; ppk-Gal4, UAS-CD8GFP / ppk-Gal4, UAS-CD8GFP. **(B) O/E Control:** w*; ppk-Gal4 / ppk-Gal4; ppk-Gal4, UAS-CD8GFP / ppk-Gal4, UAS-CD8GFP. **O/E Keap1-HA:** w*; ppk-Gal4, UAS-Keap1-HA / ppk-Gal4, UAS-Keap1-HA; ppk-Gal4, UAS-CD8GFP / ppk-Gal4, UAS-CD8GFP. **O/E Keap1:** w*; ppk-Gal4, UAS-CD8GFP / ppk-Gal4, UAS-CD8GFP; UAS-Keap1 / UAS-Keap1. **(C) Ctrl (FRT82B):** w*; ppk-Gal4, UAS-mCD8GFP, SOP-flp / +; FRT82B / FRT82B, tubP-Gal80. **cnc^{1223}:** w*; ppk-Gal4, UAS-mCD8GFP, SOP-flp / +; FRT82B, cnc^{1223}/ FRT82B, tubP-Gal80. **cnc^{1223} + O/E Keap1-HA:** w*; ppk-Gal4, UAS-Keap1-HA / ppk-Gal4, UAS-mCD8GFP, SOP-flp; FRT82B, cnc^{1223} / FRT82B, tubP-Gal80. **(D)** w*; UAS-CL1-GFP / UAS-CL1-GFP; ppk-Gal4, UAS-mCD8-mCherry / ppk-Gal4, UAS-mCD8-mCherry. **(E) Ctrl RNAi:** w*; UAS-CL1-GFP / ppk-Gal4, UAS-Dcr2; ppk-Gal4, UAS-mCD8-mCherry / UAS-Control RNAi. **cnc RNAi #1:** w*; UAS-CL1-GFP / ppk-Gal4, UAS-Dcr2; ppk-Gal4, UAS-mCD8-mCherry / UAS-cnc RNAi #1. **cnc RNAi #2:** w*; UAS-CL1-GFP / UAS-cnc RNAi #2; ppk-Gal4, UAS-mCD8-mCherry / ppk-Gal4, UAS-mCD8-mCherry. **(F) O/E Control:** w*; UAS-CL1-GFP / +; ppk-Gal4, UAS-mCD8-mCherry / UAS-Mical^{NT}. **O/E CncC:** w*; UAS-CL1-GFP / +; ppk-Gal4, UAS-mCD8-mCherry / UAS-CncC. **O/E CncA:** w*; UAS-CL1-GFP / +; ppk-Gal4, UAS-mCD8-mCherry / UAS-CncA. **(G)** w*; ppk-Gal4, UAS-mCD8GFP, UAS-Dcr2 / rpn6-lacZ; UAS-Control RNAi / +. **(H) Ctrl RNAi:** w*; ppk-Gal4, UAS-mCD8GFP, UAS-Dcr2 / rpn6-lacZ; UAS-Control RNAi / +. **cnc RNAi #1:** w*; ppk-Gal4, UAS-mCD8GFP, UAS-Dcr2 / rpn6-lacZ; UAS-cnc RNAi #1 / +. **(I) O/E Control:** w*; ppk-Gal4, UAS-mCD8GFP / rpn6-lacZ; UAS-Mical^{NT} / +. **O/E CncC:** w*; ppk-Gal4, UAS-mCD8GFP / rpn6-lacZ; UAS-CncC / +. **(J) Ctrl RNAi:** w*; ppk-Gal4, UAS-mCD8GFP, UAS-Dcr2 / rpn6-lacZ; UAS-Control RNAi / +. **EcR RNAi:** w*; ppk-Gal4, UAS-mCD8GFP, UAS-Dcr2 / rpn6-lacZ; UAS-EcR RNAi / +.

Figure S2**: (A)** w*; **UAS-CncA:** ppk-Gal4 / +; ppk-Gal4, UAS-CD8GFP / UAS-CncA. **UAS-CncB**: w*; ppk-Gal4 / UAS-CncB; ppk-Gal4, UAS-CD8GFP / +. **UAS-CncC**: w*; ppk-Gal4 / +; ppk-Gal4, UAS-CD8GFP / UAS-CncC. **UAS-CncC$^{\Delta A}$:** w*; ppk-Gal4 / UAS-CncC$^{\Delta A}$; ppk-Gal4, UAS-CD8GFP / +. **UAS-CncC$^{\Delta B}$:** w*; ppk-Gal4 / UAS-CncC$^{\Delta B}$; ppk-Gal4, UAS-CD8GFP / +. **UAS-CncC$^{\Delta DLG+ETGE}$:** w*; ppk-Gal4 / UAS-CncC$^{\Delta DLG+ETGE}$; ppk-Gal4, UAS-CD8GFP / +. **(B) O/E Control:** w*; ppk-Gal4 / ppk-Gal4; ppk-Gal4, UAS-mCD8GFP / ppk-Gal4, UAS-mCD8GFP. **O/E CncA:** w*; ppk-Gal4 / +; ppk-Gal4, UAS-mCD8GFP / UAS-CncA-HA. **O/E CncB:** w*; ppk-Gal4 / UAS-CncB; ppk-Gal4, UAS-mCD8GFP / +. **O/E CncC:** w*; ppk-Gal4 / +; ppk-Gal4, UAS-mCD8GFP / UAS-CncC. **(C) Control (FRT82B):** w*; ppk-Gal4, UAS-mCD8GFP, SOP-flp / +; FRT82B / FRT82B, tubP-Gal80. **cnc^{1223}:** w*; ppk-Gal4, UAS-mCD8GFP, SOP-flp / +; FRT82B, cnc^{1223}/ FRT82B, tubP-Gal80. **cnc^{VL110}:** w*; ppk-Gal4, UAS-mCD8GFP, SOP-flp / +; FRT82B, cnc^{VL110} / FRT82B, tubP-Gal80. **cnc RNAi #2:** w*; UAS-cnc RNAi #2 / UAS-cnc RNAi #2; ppk-Gal4, UAS-CD8GFP / ppk-Gal4, UAS-CD8GFP. **O/E Keap1-HA:** w*; ppk-Gal4 / UAS-Keap1-HA; ppk-Gal4, UAS-CD8GFP / +. **keap1^{036}:** w*; ppk-Gal4, UAS-mCD8GFP, SOP-flp / +; FRT82B, keap1^{036}/ FRT82B, tubP-Gal80.

Figure S3**: (A) Control:** w*; ppk-Gal4 / + ; ppk-Gal4, UAS-CD8GFP / UAS-Mical^{NT}. **O/E Mafs-HA:** w*; ppk-Gal4 / + ; ppk-Gal4, UAS-CD8GFP / UAS-Mafs-HA. **(B) Control:** w*; ppk-Gal4 / + ; ppk-Gal4, UAS-CD8GFP / UAS-Mical^{NT}. **O/E Mafs-HA:** w*; ppk-Gal4 / + ; ppk-Gal4, UAS-CD8GFP / UAS-Mafs-HA. **(C) Control:** w*;; ppk-Gal4, UAS-CD8GFP / ppk-Gal4, UAS-CD8GFP. **O/E CncC:** w*; ppk-Gal4 / + ; ppk-Gal4, UAS-CD8GFP / UAS-CncC. **keap1^{036}:** w*; ppk-Gal4, UAS-mCD8GFP, SOP-flp / +; FRT82B, keap1^{036}/ FRT82B, tubP-Gal80.

Figure S4**: (A) O/E Control:** w*; gstD-lacZ / +; ppk-Gal4, UAS-CD8GFP / UAS-Mical^{NT}. **O/E CncC:** w*; gstD-lacZ / + ; ppk-Gal4, UAS-CD8GFP / UAS-CncC. **(B) O/E Control:** w*; gstD-lacZ / +; ppk-Gal4, UAS-CD8GFP / UAS-Mical^{NT}. **O/E CncA:** w*; gstD-lacZ / +; ppk-Gal4, UAS-CD8GFP / UAS-CncA. **(C) Ctrl RNAi:** w*; gstD-lacZ / ppk-Gal4, UAS-CD8GFP, UAS-Dcr2; ppk-Gal4, UAS-CD8GFP / UAS-Control RNAi. **mical RNAi:** w*; gstD-lacZ / ppk-Gal4, UAS-CD8GFP, UAS-Dcr2; ppk-Gal4, UAS-CD8GFP / UAS-mical RNAi.

Figure S5**: (A) Ctrl RNAi:** w*; ppk-Gal4, UAS-CD8GFP, UAS-Dcr2 / ppk-Gal4, UAS-CD8GFP, UAS-Dcr2; UAS-Control RNAi / UAS-Control RNAi. **cnc RNAi #1:** w*; ppk-Gal4, UAS-mCD8GFP, UAS-Dcr2 / ppk-Gal4, UAS-mCD8GFP, UAS-Dcr2; UAS-cnc RNAi #1 / UAS-cnc RNAi #1. **(B) O/E Control** w*; ppk-Gal4, UAS-mCD8GFP / ppk-Gal4, UAS-mCD8GFP; UAS-Mical^{NT} / UAS-Mical^{NT}. **O/E CncC:** w*; ppk-Gal4, UAS-mCD8GFP / ppk-Gal4, UAS-mCD8GFP; UAS-CncC / UAS-CncC. **(C) O/E Control**: w*; ppk-Gal4, UAS-CD8GFP / ppk-Gal4, UAS-CD8GFP; UAS-Mical^{NT} / UAS-Mical^{NT}. **O/E Keap1:** w*; ppk-Gal4, UAS-CD8GFP / ppk-Gal4, UAS-CD8GFP; UAS-Keap1 / UAS-Keap1. **(D) Ctrl RNAi:** w*; ppk-Gal4, UAS-CD8GFP / +; UAS-Dcr2 / UAS-Control RNAi. **imp-β RNAi (#1):** w*; ppk-Gal4, UAS-CD8GFP / +; UAS-Dcr2 / UAS-imp-β RNAi #1. **imp-β RNAi (#2):** w*; ppk-Gal4, UAS-CD8GFP / +; UAS-Dcr2 / UAS-imp-β RNAi #2. **(E) Ctrl RNAi:** w*; w*; ppk-Gal4, UAS-CD8GFP / +; UAS-Dcr2 / UAS-Control RNAi. **EcR RNAi:** w*; ppk-Gal4, UAS-CD8GFP / +; UAS-Dcr2 / UAS-EcR RNAi. **usp RNAi:** w*; ppk-Gal4, UAS-CD8GFP / +; UAS-Dcr2 / UAS-usp RNAi. **(F) Ctrl RNAi:** w*; ppk-Gal4, UAS-CD8GFP, UAS-Dcr2 / ppk-Gal4, UAS-CD8GFP, UAS-Dcr2; UAS-Control RNAi / UAS-Control RNAi. **mical RNAi:** w*; ppk-Gal4, UAS-CD8GFP, UAS-Dcr2 / ppk-Gal4, UAS-CD8GFP, UAS-Dcr2; UAS-mical RNAi / UAS-mical RNAi.

Figure S6**: (A) UAS-Control:** w*; ppk-Gal4 / +; ppk-Gal4, UAS-CD8GFP / UAS-Mical^{NT}. **UAS-Sod1:** w*; ppk-Gal4 / UAS-Sod1; ppk-Gal4, UAS-CD8GFP / +. **UAS-Sod2:** w*; ppk-Gal4 / UAS-Sod2; ppk-Gal4, UAS-CD8GFP / +. **UAS-hSod1:** w*; ppk-Gal4 / +; ppk-Gal4, UAS-CD8GFP / UAS-hSod1. **UAS-Catalase:** w*; ppk-Gal4 / UAS-Catalase; ppk-Gal4, UAS-CD8GFP / +.

UAS-Jafrac1: w*; ppk-Gal4 / UAS-Jafrac1; ppk-Gal4, UAS-CD8GFP / +. **UAS-Gclc:** w*; ppk-Gal4 / UAS-Gclc; ppk-Gal4, UAS-CD8GFP / +. **UAS-Gclm:** w*; ppk-Gal4 / UAS-Gclm; ppk-Gal4, UAS-CD8GFP / +. **(B) Control (FRT82B):** w*; ppk-Gal4, UAS-mCD8GFP, SOP-flp / +; FRT82B / FRT82B, tubP-Gal80. **sod1^{n1}:** w*; ppk-Gal4, UAS-mCD8GFP / +; sod^{n1} / sod^{n1}. **sod2$^{\Delta 02}$/ sod2^{n283}:** w*; ppk-Gal4, UAS-mCD8GFP / +; sod2$^{\Delta 02}$/sod2^{n283}. **cat^{n1}/cat^{n4}:** w*; ppk-Gal4, UAS-mCD8GFP / +; cat^{n1}/cat^{n4}. **ja-frac1^{KG05372}:** jafrac1^{KG05372} / Y; ppk-Gal4 / +; ppk-Gal4, UAS-mCD8GFP / +. **(C) ND-42 RNAi #1:** w*; ppk-Gal4, UAS-mCD8GFP / ND-42 RNAi #1; UAS-Dcr2 / +. **ND-42 RNAi #2:** w*; ppk-Gal4, UAS-mCD8GFP / +; UAS-Dcr2 / ND-42 RNAi #2. **ND-75 RNAi:** w*; ppk-Gal4, UAS-mCD8GFP / +; UAS-Dcr2/ ND-75 RNAi. **aats-met^{FB}:** w*; ppk-Gal4, UAS-mCD8GFP, SOP-flp / +; FRT82B, aats-met^{FB} / FRT82B, tubP-Gal80. **marf^{B}:** w*, marf^{B}, FRT19A / w*, tubP-Gal80, FRT19A; ppk-Gal4, UAS-mCD8GFP, SOP-flp / +.

Figure S7**: (A) Control:** w*; FRTG13 / FRTG13, tubP-Gal80; ppk-Gal4, UAS-mCD8GFP, SOP-flp / +. **mafs$^{9-1}$:** w*; FRTG13, mafs$^{9-1}$ / FRTG13, tubP-Gal80; ppk-Gal4, UAS-mCD8GFP, SOP-flp / +. **mov34 RNAi:** w*, UAS-mov34 RNAi / Y; ppk-Gal4, UAS-mCD8GFP / +; UAS-Dcr2 / +. **rpn7 RNAi:** w*; ppk-Gal4, UAS-mCD8GFP / +; UAS-Dcr2 / UAS-rpn7 RNAi. **(B) Ctrl RNAi:** w*; ppk-Gal4, UAS-mCD8GFP / +; UAS-Dcr2 / UAS-Control RNAi. **mov34 RNAi:** w*, UAS-mov34 RNAi / Y; ppk-Gal4, UAS-mCD8GFP / +; UAS-Dcr2 / +. **rpn7 RNAi:** w*; ppk-Gal4, UAS-mCD8GFP / +; UAS-Dcr2 / UAS-rpn7 RNAi. **(C) Ctrl RNAi:** w*, elav-Gal4 / Y; ; UAS-Control RNAi / UAS-Dcr2. **cnc RNAi #1:** w*, elav-Gal4 / Y; ; UAS-cnc RNAi #1 / UAS-Dcr2. **(D) cnc-i #1 + UAS-Control:** w*; ppk-Gal4, UAS-mCD8GFP, UAS-Dcr2 / +; UAS-cnc RNAi #1 / UAS-Mical^{NT}. **cnc-i #1 + UAS-Prosβ5-RFP:** w*; ppk-Gal4, UAS-mCD8GFP, UAS-Dcr2 / +; UAS-cnc RNAi #1 / UAS-Prosβ5-RFP. **(E) cnc-i #1 + UAS-control**: w*; ppk-Gal4, UAS-mCD8GFP, UAS-Dcr2 / +; UAS-cnc RNAi #1 / UAS-Mical^{NT}. **cnc-i #1 + UAS-Sod1**: w*; ppk-Gal4, UAS-mCD8GFP, UAS-Dcr2 / UAS-Sod1; UAS-cnc RNAi #1 / +. **cnc-i #1 + UAS-Catalase**: w*; ppk-Gal4, UAS-mCD8GFP, UAS-Dcr2 / UAS-Catalase; UAS-cnc RNAi #1 / +. **cnc-i #1 + UAS-Jafrac1:** w*; ppk-Gal4, UAS-mCD8GFP, UAS-Dcr2 / UAS-Jafrac1; UAS-cnc RNAi #1 / +. **(F) O/E Control** w*; ppk-Gal4, UAS-mCD8GFP / rpn6-lacZ; UAS-Mical^{NT} / +. **O/E CncC:** w*; ppk-Gal4, UAS-mCD8GFP / rpn6-lacZ; UAS-CncC / +. **(G) Ctrl RNAi:** w*; ppk-Gal4, UAS-mCD8GFP, UAS-Dcr2 / rpn6-lacZ; UAS-Control RNAi / +. **sox14 RNAi:** w*; ppk-Gal4, UAS-mCD8GFP, UAS-Dcr2 / rpn6-lacZ; UAS-sox14 RNAi / +.

METHOD DETAILS

Fly Strains

UAS-mical$^{N\text{-}ter}$ (Terman et al., 2002), *ppk-Gal4* on II and III chromosome (Grueber et al., 2003), *SOP-flp* (#42) (Matsubara et al., 2011), *cnc^{K6}*, *cnc^{VL110}* (Veraksa et al., 2000), *UAS-Keap1, UAS-Keap1-HA*, *keap1^{036}*, *gstD1-LacZ*, *UAS-CncC* (Sykiotis and Bohmann, 2008), *UAS-CncB* (Veraksa et al., 2000), *UAS-Jafrac1* (DeGennaro et al., 2011; Hochmuth et al., 2011); *UAS-Gclm*, *UAS-Gclc* (Orr et al., 2005), *UAS-Prosβ5-RFP* (Kreko-Pierce and Eaton, 2017), *UAS-Sox14* (Kirilly et al., 2009), *UAS-CL1-GFP* (Pandey et al., 2007), *cnc^{1223}*, *mafs$^{9-1}$*, and *mafs$^{8-3}$* (this study).

The following stocks were obtained from Bloomington Stock Centre (BSC): *UAS-mCD8::GFP, FRTG13, FRT82B, UAS-Dicer2, tubP-Gal80, elav-Gal4^{C155}* (BL#458), *cnc* RNAi #2 (BL#40854), *rpn7* RNAi (BL#34787), *keap1* RNAi #2 (BL#40932), *UAS-EcR^{DN}* (BL#6872), *imp-β* RNAi (#1) (BL27567), *imp-β* RNAi (#2) (BL31242), *Jafrac1^{KG05372}* (BL#14440), *sod1^{n1}* (BL#24492), *sod2$^{\Delta 02}$* (BL#27643), *sod2^{n283}* (BL#34060), *UAS-Sod1* (BL#33605), *UAS-Sod2* (BL#24494), *UAS-hSod1* (BL#33606), *marf^{B}* (BL#67154), *aats-met^{FB}* (BL#39747), *UAS-Catalase* (BL#24621) and *rpn6-lacZ* (*rpn6^{k00103},* BL#10465).

The following stocks were obtained from the Vienna *Drosophila* RNAi Centre (VDRC): *cnc* RNAi #1 (v37674), *cnc RNAi #3* (v101235), *keap1* RNAi #1 (v330323), *usp* RNAi (v16893), *sox14* RNAi (v10856), *mical* RNAi (v46097) and *mov34* RNAi (v26183).

The following stocks were obtained from FlyORF: *UAS-CncA-HA* (F000602), and *UAS-Mafs-HA* (F000012).

The following stocks were obtained from the Kyoto Stock Center DGRC: *cat^{n1}* (#107554), and *cat^{n4}* (#101586).

The following stocks were obtained from the National Institute of Genetics (NIG), Japan: *ND-42* RNAi #1 (6343R-1) and #2 (6343R-2), and *ND-75* RNAi (2286-2).

EMS Mutagenesis

Isogenized *w*;;FRT82B* male flies were treated with 25 mM EMS. Mutant chromosomes were balanced over the TM6B, Tb balancer chromosome. Lethal or semi-lethal lines were then selected for the following MARCM analysis.

Generation of various cnc transgenes

The *cncC* full-length cDNA was PCR amplified from the *UAS-cncC* transgene and inserted into pENTR/D-TOPO (Invitrogen). CncC deletions were generated by site mutagenesis (Agilent Tech.). The GATEWAY pTW or pTVW containing the cDNA of various CncC deletions were constructed by LR reaction (Invitrogen) and multiple transgenic lines were established by the Bestgene Inc.

Generation of mafs mutants via CRISPR/Cas9 technology

Two different guide RNAs (gRNAs) targeting *mafs* exons were cloned into the pCFD4 vector following the standard procedures (Port et al., 2014). The primer set was used as follows: 5′-GCACCACTTTCGCCATGTCCAATTCCGGATATTACCGAT GACGATTTGGTG AGCATTTCGGTAAGGGATCTTAATCGGACCCTCAAGAT GCGTGGCCTGAACCGCGAGGAGATCGTTCGGATGAA-3′, 5′-CGTGGT GAA AGCGGTACAGGTTAAGGCCTATAATGGCTACTGCTAAACCACTCGTA AAG CCATTCCCTAGAATTAGCCTGGGAGTTCTAC GCACCGGACTTGGCGCTCCTCTAGCAAGCCTACTT-3′. Transgenic flies were generated by BestGene Inc and crossed with

nanos-Cas9 flies to generate mutant *mafs* lines. Lethal mutants were isolated, and the indels were confirmed by PCR sequencing. Embryo microinjection services were provided by BestGene Inc.

Generation of anti-CncC antibody

Two CncC fragments (P2, amino acid 429–578; P4, amino acid 884-1133) were expressed using the 6XHis expression vector (pQE30, QIAGEN) and the GST expression vector (pGEX 4T-1, Pharmacia), respectively. The purified proteins were used to immunize mice to generate antibodies against CncC. The specificity of the antibody against the CncC region (P2) was determined using *cnc* RNAi knockdown and overexpression in ddaC neurons.

Immunohistochemistry and antibodies

The following primary antibodies were used for immunohistochemistry at the indicated dilutions: mouse anti-CncC (P2) (1:500; this study), mouse anti-CncC (P4) (1:500; this study), mouse anti-β-Galactosidase (1:1000; Promega, Cat#Z378A), mouse anti-Ubiquitin (1:500; FK2, Enzo Life Sciences BML-PW8810), rat anti-HA (1:250; Roche, Cat#11867423001), mouse anti-EcR-B1 (1:50; DSHB, AD4.4), and guinea pig anti-Mical (1:500; Yu lab). Cy3- or Cy5-conjugated secondary antibodies (Jackson Laboratories) were used at 1:500 dilution. For immunostaining, staged pupae or larvae were dissected in cold PBS and fixed with 4% formaldehyde for 20 min. The control and mutant samples were incubated simultaneously in the same tubes. Mounting was performed in Vecta-Shield mounting medium, and the samples were directly visualized by the Olympus FV3000 confocal microscopy. The images were taken at the same confocal setting, and the data were processed in parallel. The non-blind experiments were repeated for three times.

Live imaging analysis

To image the dendrites of da sensory neurons at 3rd instar (wL3), WP or 6 h APF, larvae or pupae were collected at 6-h intervals and briefly rinsed with PBS buffer, followed by immersion with 80% glycerol. To image da neurons at 16 h APF, pupal cases were removed before being mounted with 80% glycerol. Images of da neurons were acquired on Leica SPE2 laser confocal microscope.

MARCM analysis of da sensory neurons

MARCM clonal analysis, dendrite imaging, and branch quantification were carried out as previously described (Kirilly et al., 2009). ddaC clones were identified based on their location and morphology at the WP stage. ddaC neurons were examined for dendrite pruning defects at 6 or 16 h APF.

Quantitative real-time PCR (Q-PCR)

At least three independent experiments were conducted in triplicates using Maxima SYBR Green/ROX qPCR Master Mix (Fermentas) and 7900HT Fast Real-time PCR system (Applied Biosystems) according to manufacturer's recommendations. *actin5C* was used as an internal control gene. Results were normalized to controls indicated. Error bars represent standard deviation for technical triplicates of a single experiment. See Table S1 for primers used.

Quantification of dendrites

Live confocal images of da neurons expressing *mCD8-GFP* were conducted at WP stage or 16 h APF. Dorsal is up in all images. For wild-type or mutant ddaC neurons, the percentages of severing defects and fragmentation defects were quantified in a 275 μm x 275 μm region of the dorsal dendritic area, originating from the abdominal segments 2-4. The non-blind experiments were repeated for three times. The categorization of severed of fragmented dendrites was determined manually, based on their morphology. The severing defect was determined by the presence of dendrites (at least 100 μm long) that remain attached to the soma at 16 h APF, whereas dendrite fragmentation defect is referred to as the presence of dendrite branches (at least 50 μm long) near the ddaC territory but have been severed from their proximal parts at 16 h APF (Figure 1A). Total length of unpruned dendrites was measured in a 275 μm x 275 μm region of the dorsal dendritic field using ImageJ. The semi-automated tracing tool, simple neurite tracer plug-in in ImageJ (Under Plugins→Segmentation), was used to measure the length of unpruned dendrites in ddaC neurons. The measured lengths of dendrites in inches were converted to micrometers.

$$\frac{Sum\ of\ dendritic\ length\ (in\ inches)}{Image\ size\ (in\ inches)} \times Image\ size\ (in\ \mu m)$$

The number of neurons (n) examined in each group is shown on the bars. Plots of average length and SEM were generated using GraphPad Prism software.

Quantification of immunostaining

Images were taken from projected z stacks (at 1.5 μm intervals) to cover the entire da sensory neurons using the Olympus FV3000 confocal microscopy. To measure the fluorescence intensities, cell nuclei (CncC/*gstD-lacZ*/EcR-B1/*rpn6-lacZ* immunostaining) or whole soma (Ub/Mical immunostaining and CL1-GFP live imaging) contours were drawn on the appropriate fluorescent channel based on the GFP (CncC/*gstD1-lacZ*/EcR-B1/Mical/Ub/*rpn6-lacZ*) or RFP (CL1-GFP) channel in ImageJ. To quantify the

fluorescence intensities of *gstD1-lacZ*, Ub and CL1-GFP, after subtracting the background (Rolling Ball Radius = 50) on the entire image of that channel, the mean gray value in the marked area in ddaC was measured. To quantify the fluorescence intensities of EcR-B1, Mical, CncC and *rpn6-lacZ* after subtracting the background (Rolling Ball Radius = 50) on the entire image of that channel, the mean gray value in the marked area in ddaC and ddaE on the same images were measured and their ratio were calculated. The values were normalized to the corresponding average control values and subjected to statistical analysis for comparison between different conditions. Graphs display the average values of the normalized intensities (*gstD1-lacZ*/CL1-GFP/Ub/*rpn6-lacZ*) or ddaC/ddaE ratios (EcR-B1/Mical/CncC/*rpn6-lacZ*) and the standard error of the mean (SEM) normalized to the controls. The non-blind experiments were repeated for three times. The number of ddaC neurons (n) examined in each group is shown on the bars. Insets show the ddaC neurons labeled by *ppk-Gal4*-driven mCD8-GFP expression or HRP-Cy5 staining. Dorsal is up in all images.

QUANTIFICATION AND STATISTICAL ANALYSIS

For pairwise comparison, Two-tailed Student's t test was used to determine statistical significance. For multiple-group comparison, One-way ANOVA and Bonferroni test was utilized to determine significance. Error bars in all graphs represent SEM from three independent experiments. Statistical significance was defined as ****$p < 0.0001$, ***$p < 0.001$, **$p < 0.01$, *$p < 0.05$, ns, not significant. The number of neurons (n) in each group is shown on the bars.